JOURNAL OF PETROLOGY | VOLUME 51 | NUMBER 9 | PAGES 1891–1912 | 2010 | doi:10.1093/petrology/egq042

A Felsic End to Bushveld Differentiation

JILL A. VANTONGEREN[1,2]*, EDMOND A. MATHEZ[2] AND PETER B. KELEMEN[1]

[1]LAMONT–DOHERTY EARTH OBSERVATORY, COLUMBIA UNIVERSITY, 61 RT. 9W, PO BOX 1000, PALISADES, NY 10964, USA

[2]AMERICAN MUSEUM OF NATURAL HISTORY, NEW YORK, NY 10024, USA

RECEIVED NOVEMBER 3, 2009; ACCEPTED JULY 5, 2010
ADVANCE ACCESS PUBLICATION AUGUST 2, 2010

The similarities in age (c. 2·06 Ga) and isotopic composition of the Bushveld Igneous Complex and the overlying Rooiberg Group felsic volcanic rocks suggest the possibility that the two are cogenetic. To investigate this possibility we derive a robust new estimate of the major and trace element bulk composition of the Bushveld Upper Zone and Upper Main Zone (UUMZ). Using MELTS thermodynamic modeling, we show that this composition fails to reproduce fundamental features of the cumulate sequence, such as the presence of primary orthopyroxene at the base of the magma column. We investigate the possibility that some amount of evolved magma escaped from the magma chamber and derive a new estimate of the UUMZ parent magma composition that reproduces generally the observed cumulate sequence. Our results constrain the amount and composition of the escaped magma and provide evidence of a genetic link between the UUMZ of the Bushveld layered series and the felsic volcanic rocks immediately overlying it. We conclude that between 15 and 25% of the original magma volume was expelled and is manifest either as part of the upper Rooiberg Group lava sequence or the Rashoop Granophyre (distinction is hindered by their almost identical major and trace element compositions). A parent magma in which 15–25% Rooiberg or Rashoop material is added back to the extant cumulate sequence is initially saturated in orthopyroxene and is in major and trace element equilibrium with the phases at the base of the UUMZ.

KEY WORDS: *Bushveld Complex; MELTS; parent magma; Rooiberg lavas; Rashoop Granophyre; UUMZ*

INTRODUCTION

The body of rock forming the combined Upper Zone and Upper Main Zone of the Bushveld Complex (hereafter referred to as the UUMZ) is commonly thought to represent the last pulse of magma injected into the Bushveld magma chamber. The upward progression in this unit of more chemically and mineralogically evolved rocks is traditionally regarded as the result of closed-system fractional crystallization. Some researchers have hypothesized, however, that a significant proportion of the magma now represented by the UUMZ escaped from the original chamber (Cawthorn & Walraven, 1998). Despite the relevance of this hypothesis to the source, evolution, and nature of emplacement of the Bushveld Complex, no attempts to quantify the amount or composition of escaped magma have been made, and no rocks that might represent that magma have been identified.

To determine if significant quantities of magma were expelled from the UUMZ, one must deduce the original composition of the magma from which the extant rock column crystallized. With the assumption (explored below) that the UUMZ is a cumulate sequence formed essentially from a single pulse of magma, the rocks provide three constraints on the parent magma composition: (1) it must initially be saturated in the phases present at the base of the UUMZ, namely orthopyroxene ± plagioclase ± clinopyroxene; (2) it must be in equilibrium with the observed mineral compositions at the base; (3) it must crystallize in a paragenetic sequence consistent with the observed stratigraphic succession of rock types. To date, no parent magma that satisfies any of these three basic constraints has been identified for the UUMZ.

Thus, there remain several fundamental questions about the formation and evolution of the Bushveld UUMZ: what was its parent magma composition, how much magma was lost during crystallization, what was

*Corresponding author. E-mail: jvantong@ldeo.columbia.edu

the composition of the lost magma, and where are the rocks representing this material? To address these questions, we first calculate a bulk composition for the UUMZ. We then derive a new estimate of the parent magma by exploring the relationship between the UUMZ cumulate sequence and the felsic rocks directly overlying it, namely the Rooiberg Group lavas and the Rashoop Granophyre Suite. We focus specifically on the potential for, and magnitude of, expelled magma using MELTS thermodynamic modeling. As an independent test of our results, we reconstruct major and trace element liquid compositions from the observed cumulus mineral compositions at the base of the UUMZ.

GEOLOGICAL AND GEOCHEMICAL RELATIONS

The Rustenburg Layered Suite (RLS)

The Bushveld Complex *sensu stricto* is made up of three parts: the Rustenburg Layered Suite (RLS) of ultramafic–mafic intrusive rocks, the Rashoop Granophyre Suite, and the Lebowa Granite Suite, but it excludes the Rooiberg Group lavas (SACS, 1980). The Lebowa granites are demonstrably younger than the RLS (e.g. Wilson *et al.*, 2000), and the relationship between the Rashoop Granophyre and surrounding rocks remains unclear (see below). For these reasons, we follow informal convention and use the term Bushveld Complex to mean the RLS and refer to other units by their specific names.

The Bushveld Complex crops out in east- and west-arching limbs with a total strike length of over 350 km (Fig. 1). The two limbs dip gently inward towards each other and appear to be connected at depth (Cawthorn & Webb, 2001; Webb *et al.*, 2004), implying that the main part of the Bushveld is a shallow, bowl-shaped body (Kruger, 2005). In addition, there exists a 110 km long northern limb extending north from the town of Mokopane (formerly Potgietersrus) and a mostly hidden, eroded remnant in the far west extending to the Botswana border. The northern and western limbs of the Bushveld are poorly exposed and are known from mining activity and drilling. Parts of the eastern limb, on the other hand, are well exposed as a result of the locally rugged topography. This is where the Bushveld has been mapped in some detail (e.g. Molyneux, 1970; von Gruenewaldt, 1973; Sharpe, 1981).

The UUMZ

The Main and Upper Zones in the eastern limb of the Bushveld Complex were mapped in detail by Molyneux (1970, 1974) in the Magnet Heights area and by von Gruenewaldt (1971, 1972) further to the south in the Steelpoort River valley. Additionally, Ashwal *et al.* (2005) provided a detailed description based on drill core of the Upper Zone and approximately half the Main Zone of the northern limb. The UUMZ of the western limb is known from the general descriptions of Kruger *et al.* (1987) and Tegner *et al.* (2006).

The base of the Upper Zone is formally defined as the first appearance of cumulus magnetite (SACS, 1980); however, the Bushveld magma chamber seems to have received a large influx of new magma at the level of the Pyroxenite Marker (Cawthorn *et al.*, 1991), which is a massive, 3 m thick orthopyroxenite *c.* 650 m below the first appearance of cumulus magnetite in the eastern limb (Fig. 2). At this level, initial Sr isotopic compositions decrease sharply from 0·7080 in the Main Zone below the Pyroxenite Marker to an approximately constant value of 0·7073 through the entire overlying sequence (Sharpe, 1985; Kruger *et al.*, 1987). These isotopic features, in addition to the progression of more evolved mineral compositions and assemblages (except for minor reversals—see below) from the Pyroxenite Marker upward to the roof of the Bushveld Complex, are the reasons for our delineation of the UUMZ as a coherent unit.

These observations also underlie the assumption, noted above, that the UUMZ formed by differentiation of a single magma body. This assumption may not be strictly correct, however. Ashwal *et al.* (2005) documented numerous reversals in mineral composition and density throughout the Main Zone that they attributed to small injections of new magma. They also described similar reversals in the Upper Zone, although Cawthorn & Ashwal (2009) ruled out the multiple-pulses hypothesis, at least to explain the magnetitite and associated anorthosite layers of the Upper Zone.

Regardless, although it is likely that the UUMZ was not entirely closed to small new inputs of magma during its evolution, the assumption of a closed system is valid for this study for two main reasons. First, the homogeneous bulk-rock Sr isotopic composition of the UUMZ has been interpreted to be a *c.* 50:50 mixture of resident Main Zone magma and new incoming magma (Cawthorn *et al.*, 1991). If this were correct, then any relatively massive new pulses of magma added to the UUMZ would need the exact Sr isotopic composition of this mixture, a highly fortuitous circumstance. Second, magma additions could not have been so massive compared with the resident magma as to disrupt the crystallizing phase assemblage or significantly reverse the evolving mineral compositions.

Attempts to constrain the composition of UUMZ parent magma

Cawthorn & Walraven (1998) compiled published Zr and K bulk-rock analyses of all the major layers of the Bushveld Complex. This compilation revealed that the cumulate rocks have far lower abundances of Zr and K than any proposed parent magma (Fig. 3). A straightforward

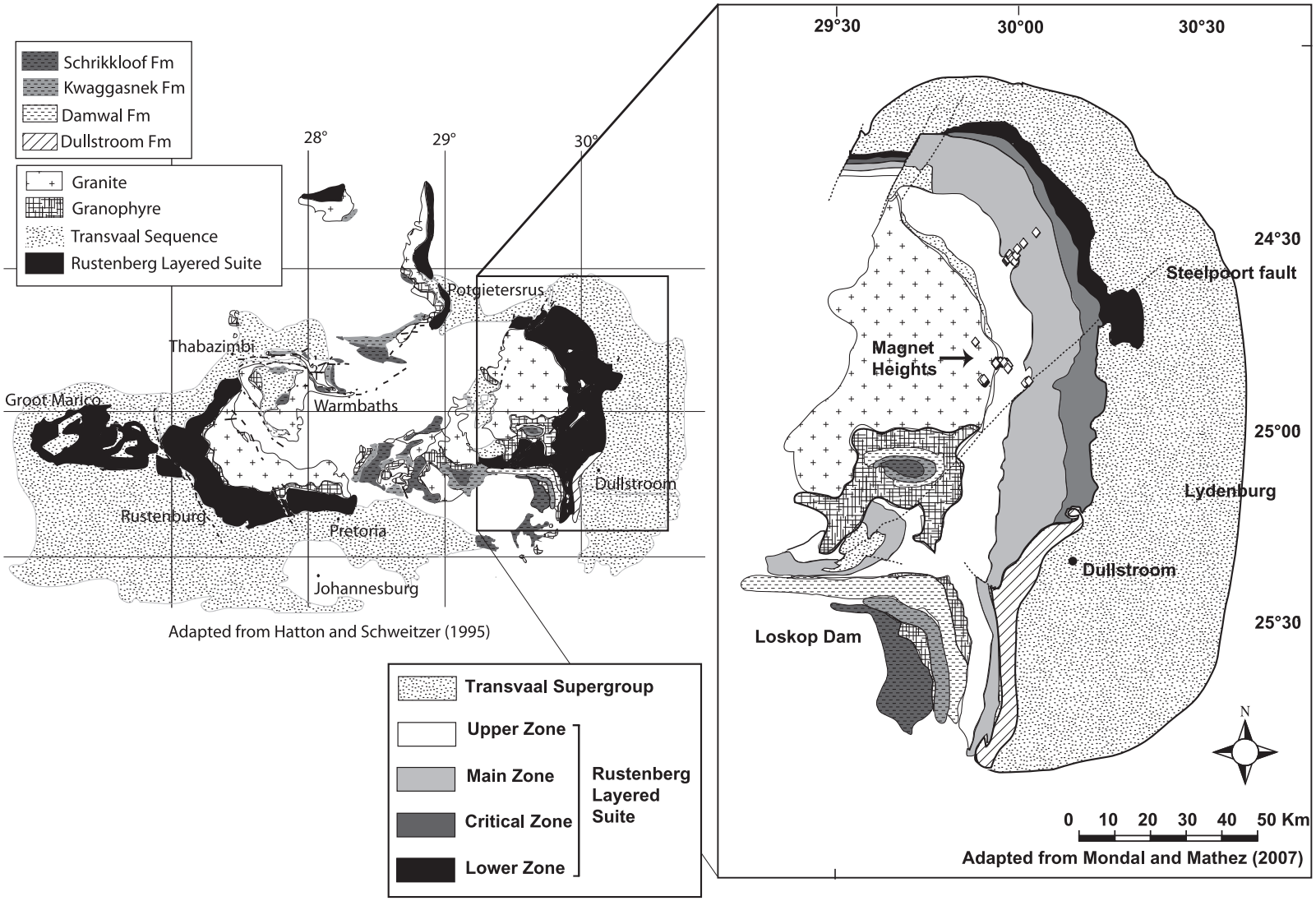

Fig. 1. Geological map of the Bushveld Complex and surrounding rocks. The regional map, which is adapted from Hatton & Schweitzer (1995), highlights the distribution and spatial relationship between the Rooiberg Group lavas and the Bushveld Complex. It should be noted that the Damwal and Dullstroom formations are present only in the eastern Bushveld. Enlargement of the eastern Bushveld adapted from Mondal & Mathez (2007). Small white diamonds indicate the locations of samples from the Main Zone and UUMZ analyzed in this study.

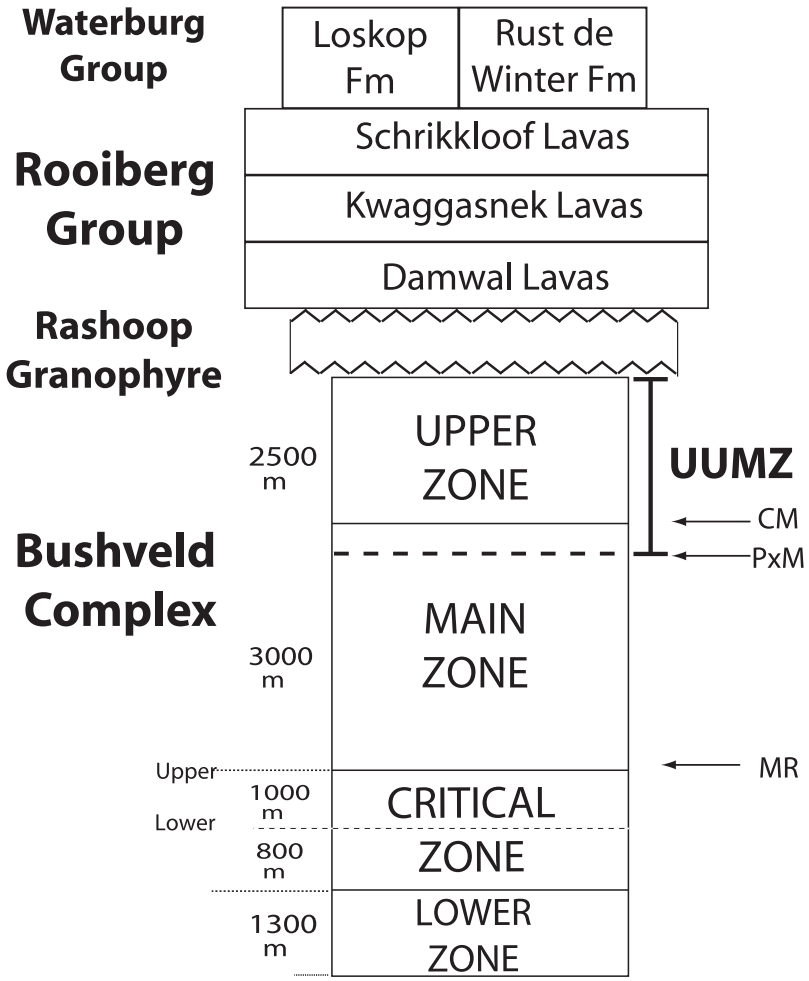

Fig. 2. Generalized stratigraphic columns of the eastern Bushveld Complex and Rooiberg Group. Rooiberg Group and Rashoop Granophyre thicknesses are not to scale.

mass balance led Cawthorn & Walraven (1998) to conclude that some amount of magma must be missing from the original magma chamber to account for the missing Zr and K. Without speculating on its composition, they estimated that the amount of expelled magma was 20–50% of that in the original chamber.

Building on this study, Tegner *et al.* (2006) attempted to estimate the UUMZ parent magma composition by adding back 20% escaped melt to the extant rock column. They derived an escaped melt composition from literature data on experimental liquids in equilibrium with olivine, clinopyroxene, plagioclase, ilmenite and magnetite—five of the seven cumulus phases near the top of the UUMZ. As shown below, however, the resulting composition cannot be the parent magma to the UUMZ because it is not initially saturated in orthopyroxene, the primary cumulus phase directly above the Pyroxenite Marker.

The roof of the Bushveld Complex

The rocks immediately overlying the Bushveld Complex include the Rooiberg Group lavas, the Rashoop Granophyre Suite, and the Lebowa Granite Suite (Figs 1 and 2). The Rooiberg Group has been subdivided into four formations (Fig. 2). At the base is the Dullstroom Formation, a sequence of mainly basaltic to andesitic lavas (Buchanan *et al.*, 1999) found only in the eastern limb (Fig. 1). The Dullstroom Formation is found almost exclusively below the Bushveld Complex, although it may also exist above the Bushveld Complex in one small area near Loskop Dam (e.g. Schweitzer *et al.*, 1995*a*). Elsewhere, the Bushveld Complex is directly overlain by the Damwal Formation (Fig. 2). The Damwal Formation consists of relatively homogeneous, low-Mg andesites and rhyolites (Schweitzer & Hatton, 1995; Schweitzer *et al.*, 1997; Buchanan *et al.*, 2002). The third and fourth layers in the

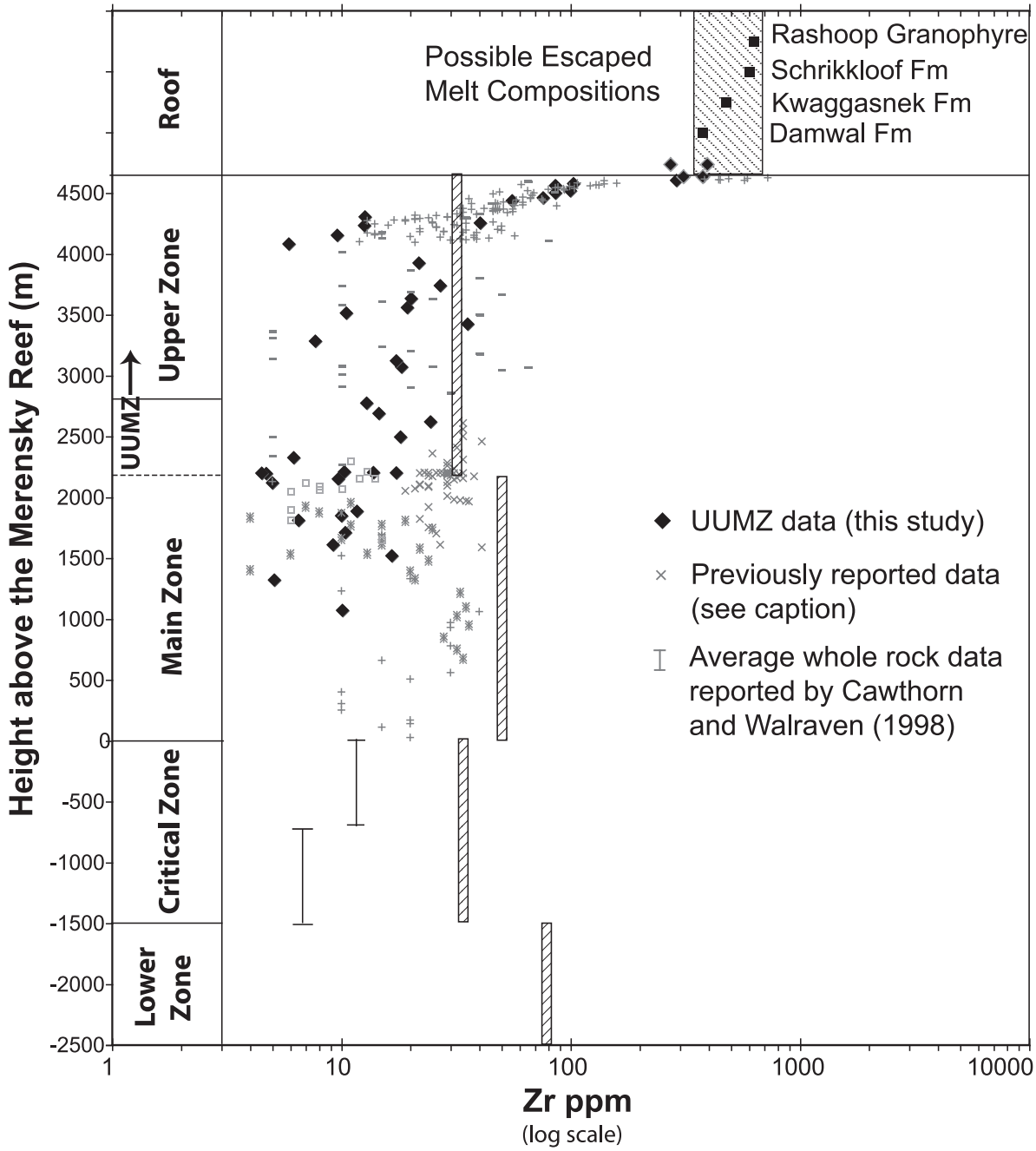

Fig. 3. Bulk-rock Zr contents of the Bushveld Complex and overlying rocks. Filled diamonds are Zr data from this study (Table 1). Small grey symbols represent Bushveld bulk-rock Zr data from Cawthorn & McCarthy (1985), Cawthorn *et al.* (1991), Bowes *et al.* (1997), Nex *et al.* (2002) and Lundgaard *et al.* (2006). Potential escaped melt compositions in filled squares are Rooiberg and Rashoop data from Schweitzer *et al.* (1997). Vertical striped bars represent estimates of parent magma composition from compilation of Cawthorn (2007).

sequence are the Kwaggasnek and Schrikkloof Formations (also referred to as the Lower and Upper Selons River Formations, and the Doornkloof and Kilpnek Formations; SACS, 1980; Twist, 1985; Schweitzer *et al.*, 1995*b*), which become progressively more rhyolitic with stratigraphic height. The Kwaggasnek and Schrikkloof Formations exist in isolated areas scattered widely across the Transvaal Basin, suggesting that they were once laterally extensive (Fig. 1).

The original extent and thickness of the Rooiberg sequence is poorly constrained because of lack of preservation and the fact that its relationship with the Rashoop

Granophyre Suite, with which it is intimately associated, is unclear. Noting the striking similarity in composition between the granophyre and the lavas, von Gruenewaldt (1972) proposed that the former represents remobilized Rooiberg roof material that was intruded into the unmelted lava sequences somewhat more distant from the contact; that is, the granophyre is completely remelted Rooiberg lava. Walraven (1985, 1987) argued that there exist within the Rooiberg sequence several different granophyres with different ages and petrogeneses, from intrusive equivalents of the Rooiberg lavas that predate the Bushveld Complex to less voluminous ones that formed when the Bushveld magma melted its Rooiberg roof. This is further complicated by the presence of granophyre between the Rooiberg lavas and the later intruding Lebowa Granites (Walraven, 1985).

Similarities of the Rooiberg and Bushveld: ages, isotopes, trace elements

Because of their ages, the magmas of the Bushveld Complex are typically thought to have intruded between the Dullstroom and the Damwal formations. In actuality, few age dates exist for either the Rooiberg or Bushveld rocks. The most precise Rooiberg dates come from Walraven (1997), who reported a Pb evaporation age of 2061 ± 2 Ma from two zircon populations separated from Kwaggasnek rhyolite, and from R. A. Armstrong *et al.* (unpublished), who obtained a thermal ionization mass spectrometry–sensitive high-resolution ion microprobe zircon U–Pb date of 2059·9 ± 1·0 Ma but provided no sample information. Additionally, a date of 2057·3 ± 3·8 Ma is frequently cited for the upper Rooiberg Group lavas from Harmer & Armstrong (2000). All dates are identical within error to a hydrothermal U–Pb cooling age of 2058·9 ± 0·8 Ma obtained from a titanite from a calcsilicate xenolith in the Bushveld Upper Zone (Buick *et al.*, 2001). These dates are not nearly as accurate as their generally high precisions would suggest, however. This is illustrated by the reliable but somewhat younger U–Pb age for zircon from the Merensky Reef of 2054 ± 1·3 Ma (Scoates & Friedman, 2008); R. A. Armstrong *et al.* (unpublished) derived a similar age for Merensky Reef zircon. Thus, the relative ages of the Upper Zone and Rooiberg lavas have yet to be definitively determined by radiometric dating techniques.

Geochemically the Rooiberg Group lavas are remarkably similar to the Bushveld Complex. The former show trace element depletions in Sr, Sc, Co, Ni, and P indicating varying degrees of fractional crystallization of plagioclase, pyroxene, olivine and apatite prior to eruption (Buchanan *et al.*, 2002)—all abundant minerals of the Upper Zone. Additionally, Sr and Nd isotopic data indicate that the compositions of Rooiberg and Bushveld rocks are similar. Using data from Sharpe (1985) and Kruger *et al.* (1987), a homogeneous average bulk-rock initial $^{87}Sr/^{86}Sr$ ratio of 0·7073* is evident throughout the UUMZ stratigraphy (*indicates the value recalculated to 2·06 Ga). The Damwal lava samples have a median $^{87}Sr/^{86}Sr$ ratio of 0·7071* (Buchanan *et al.*, 2004); because of the large range in reported values, the median value is more representative than the average for these samples. The one geologically reasonable analysis of a Kwaggasnek lava yielded a ratio of 0·7075* (Buchanan *et al.*, 2004). The Nd isotopic composition of the Rooiberg Group is better characterized than the Bushveld Complex UUMZ. In fact, the UUMZ is known from only one bulk-rock analysis, which yielded a $^{143}Nd/^{144}Nd$ ratio of 0·50965* (Tanaka & Masuda, 1982). This value is slightly higher than, but within the range of, values reported for the Damwal and Kwaggasnek lavas (Buchanan *et al.*, 2004).

Many workers have questioned the relationship between the intrusive mafic rocks of the Bushveld Complex and the lavas of the Rooiberg Group. Hatton & Schweitzer (1995) proposed a possible scenario for the contemporaneous extrusion of Rooiberg lavas and intrusion of the different zones of the Bushveld Complex. In their model, the Rooiberg lavas represent partial melts of lower crust formed as a result of the heat of the rising Bushveld diapir, with the Dullstroom lavas representing mixtures of crustal melt with an early Bushveld mafic magma and the Damwal, Kwaggasnek, and Schrikkloof lavas representing pure crustal melts expelled at various times during Bushveld magmatism. Maier *et al.* (2000) proposed a variant of this model, suggesting that all of the Rooiberg lavas formed by mixing between a mafic magma and melted lower crust. In their scenario, the increasingly rhyolitic composition of the Rooiberg lavas with stratigraphic height is the result of an increased proportion of lower crustal melt involved in the mixing.

Buchanan *et al.* (2002) showed, however, that neither of these hypotheses could account for the major and trace element geochemistry of the Rooiberg Group. Instead, they proposed that the Rooiberg lavas represent mantle-derived melts that underwent both crustal assimilation and significant differentiation in two or more shallow magma chambers. In fact, on the basis of Sr and Nd isotopic similarities, Buchanan *et al.* (2004) suggested that the Rooiberg Group lavas 'may have resided in the same magma chamber suggested as an intermediate residence for the magmas of the RLS'.

What is clear from the cumulates of the Bushveld Complex, however, is that if some amount of evolved magma escaped from the Bushveld magma chamber, it must either be manifest as some fraction of the Rooiberg lavas and/or Rashoop granophyres, or it has since been eroded away. Significant erosion can be ruled out by the preservation of the Waterburg Group sediments (2054 ± 4 Ma; Dorland *et al.*, 2006) deposited on top of, but only shortly after, the formation of the Rooiberg Group and the Bushveld Complex.

We propose that one of the shallow magma chambers invoked by Buchanan *et al.* (2004) was the Bushveld Complex itself, and specifically the UUMZ. To test this hypothesis, we present the results of MELTS thermodynamic modeling in which incremental amounts of Rooiberg lava and Rashoop granophyre are added to the bulk composition of the UUMZ to produce a viable parent magma composition. We then verify the results of the MELTS modeling by assessing major and trace element equilibrium between the proposed parent magmas and the phases at the base of the UUMZ.

METHODS

Geochemical analyses

Twenty-eight new samples collected from the UUMZ in the eastern Bushveld were analyzed by X-ray fluorescence (XRF) for bulk-rock major and trace element compositions at the Washington State University Geoanalytical Laboratory (Table 1). Because of the difficulty of calibrating XRF data at high Fe concentrations, no bulk-rock magnetitite samples were analyzed.

Electron microprobe analyses of pyroxene, plagioclase, olivine and magnetite were determined using the Cameca SX100 microprobe at the American Museum of Natural History (Fig. 4). An acceleration potential of 15 keV, beam current of 20 nA, count times of 30 s on peak and 15 s on background, and a beam diameter of 1–5 μm were used. As a check, standards were regularly reanalyzed with unknowns. Their compositions consistently reproduced to within 2σ uncertainty the known composition.

In situ laser ablation inductively coupled plasma mass spectrometry (LA-ICPMS) trace element analyses were conducted at the Lamont–Doherty Earth Observatory–American Museum of Natural History ICP-MS facility using a VG PlasmaQuad ExCell ICP-MS system equipped with a New Wave UP-193-FX excimer laser ablation system. Standards BCR, BIR and BHVO were regularly reanalyzed for continuous calibration to account for machine drift. The standard NIST612 was regularly reanalyzed as an unknown to ensure accuracy.

LA-ICPMS operating conditions for each mineral were chosen to optimize signal time and precision. For pyroxenes a spot size of 40 μm was used with an operating power of 2·2 GW/cm^2 and 10 Hz beam current. Plagioclases were analyzed with a spot size of 75 μm, 1·9 GW/cm^2 and 10 Hz. For each analysis, the location of the spot was determined with a petrographic microscope attached to the laser apparatus with both plane- and crossed-polar light capabilities. This allowed us to avoid exsolution lamellae (in the case of pyroxenes) or secondary alteration. In all cases the core of the mineral was analyzed so as to maximize the likelihood of obtaining the original igneous phase compositions. For all elements, the calibration regression had an $r^2 > 0{\cdot}99$.

Choice of basaltic liquid evolution program

To identify a parent magma in equilibrium with the phases at the base of the UUMZ, we employed the MELTS Gibbs free energy minimization algorithm of Ghiorso & Sack (1995) and the front-end application Adiabat_1ph of Smith & Asimow (2005). MELTS is calibrated on an extensive experimental database and is applicable at a range of oxygen fugacities, pressures, and initial melt compositions from basaltic to rhyolitic [although it performs best at compositions similar to mid-ocean ridge basalt (MORB)]. Although MELTS does not perfectly reproduce the liquid line of descent (see below), it is the best tool of its kind available for this study. For example, the program Comagmat (Ariskin *et al.*, 1993), which can also be used for tracking the melt composition during fractional crystallization, prompts the user to choose a low-Ca pyroxene, whereas here we seek to find a composition that distinguishes between the pyroxene crystallizing.

MELTS modeling parameters

All MELTS runs were isobaric and run via fractional crystallization in which temperature was decreased in 10 degree intervals. Crystallization was stopped when the temperature fell to 700°C.

The calculation of a crystallization sequence requires knowledge of the oxygen fugacity (fO_2). The constraint on fO_2 comes from the point at which magnetite appears in the section. Magnetite is the first oxide to crystallize in the UUMZ, which, based on the experiments of Toplis & Carroll (1995), indicates that fO_2 was likely to have been at or above the fayalite–magnetite–quartz (FMQ) buffer at this point in the crystallization sequence. Magnetite enters as a cumulus phase *c.* 650 m above the Pyroxenite Marker (27% of the extant rock column). Because of its high density relative to the liquid and all other cumulus phases, the level of the stratigraphically lowest magnetitite seam (LS1 of Molyneux, 1974) is taken to be equivalent to the point at which magnetite becomes stable in the liquid. (This is *c.* 25 m above the first appearance of cumulus magnetite in the UUMZ, but for the present purpose this difference is negligible.) An fO_2 near FMQ provides a good fit for the observed and calculated points at which magnetite appears in the crystallization sequence.

Oxygen fugacity is further constrained to have been near FMQ by the presence of fayalitic olivine in the upper portions of the extant rock column. In MELTS runs in which the fO_2 was held constant, either olivine did not appear until late in the sequence or it was entirely absent. However, fayalitic olivine (Fo < 45) enters the crystallization sequence after *c.* 50% crystallization of the extant rock column. To investigate the discrepancy, we also conducted a series of MELTS experiments allowing fO_2 to vary during crystallization. Although these runs generally did produce fayalitic olivine earlier in the

crystallization sequence, fO_2 fell to geologically unreasonable levels (FMQ − 6) as crystallization proceeded. We therefore place more confidence in, and thus report only, the results of MELTS runs in which fO_2 is fixed.

One constraint on the pressure of the UUMZ during crystallization was given by Wallmach *et al.* (1995), who calculated a pressure of <150 MPa for the formation of a calc-silicate xenolith in the UUMZ of the eastern Bushveld. The xenolith

Table 1: UUMZ bulk-rock major and trace element compositions and calculated modes

Sample no.:	B06-060	B07-007	B07-009	B06-062	B06-064	B06-065	B06-066	B06-067	B06-002	B07-057	B06-021	B07-061	B06-024	B07-004
Height (m):[1]	2200	2203	2210	2325	2495	2620	2690	2775	3070	3122	3283	3425	3515	3560
Lithology:[2]	px	px	gb	gb	gb	gb	gb	gb	px–an	mt gb	gb	mt–an	tr	mt gb
Oxide wt %														
SiO_2	53·65	52·78	51·47	52·32	51·41	51·86	52·12	51·58	52·66	46·81	46·22	50·45	42·77	46·12
TiO_2	0·28	0·28	0·18	0·16	0·22	0·26	0·21	0·20	0·22	1·85	1·63	1·30	1·51	1·95
Al_2O_3	2·61	3·89	14·97	12·68	17·36	18·17	19·37	15·47	25·61	18·15	15·79	24·34	16·10	15·29
FeO*	14·56	11·66	7·21	9·05	6·15	6·48	5·86	7·84	3·43	13·50	15·34	6·18	20·59	16·08
MnO	0·33	0·28	0·17	0·21	0·14	0·14	0·13	0·19	0·06	0·14	0·19	0·06	0·22	0·18
MgO	22·52	19·74	11·79	15·00	8·76	7·60	6·31	8·96	1·58	4·33	6·18	0·42	8·29	6·10
CaO	5·27	9·90	12·00	8·86	13·43	12·74	13·33	12·29	11·76	10·40	9·91	9·32	6·76	10·39
Na_2O	0·31	0·41	1·35	1·14	1·78	2·03	2·28	1·99	3·80	2·83	2·31	4·19	2·53	2·43
K_2O	0·09	0·04	0·11	0·09	0·23	0·31	0·23	0·16	0·38	0·27	0·19	0·96	0·22	0·29
P_2O_5	0·01	0·01	0·01	0·01	0·02	0·02	0·02	0·01	0·01	0·02	0·01	0·01	0·02	0·02
Sum	99·62	98·97	99·26	99·52	99·51	99·61	99·86	98·70	99·50	98·33	97·77	97·21	99·01	98·85
ppm														
Ni	442·2	390·0	234·5	289·6	156·2	131·6	108·1	133·1	17·6	113·1	117·9	0·0	33·6	54·1
Cr	830·0	1173·1	656·1	476·0	344·9	287·8	109·7	33·3	13·0	0·2	4·1	71·9	5·3	9·2
Sc	49·4	57·8	34·5	31·4	35·4	33·4	32·6	44·3	10·4	30·5	36·3	6·3	10·2	41·5
V	189·2	197·6	120·4	107·9	126·4	136·9	141·1	160·8	68·8	825·4	774·4	243·3	262·8	480·3
Ba	20·4	13·2	38·6	36·8	74·3	107·9	81·2	52·8	148·4	117·1	84·2	272·4	103·7	116·2
Rb	2·6	0·5	1·5	1·5	4·1	6·0	4·1	3·0	4·8	3·5	1·8	23·5	2·4	4·5
Sr	22·7	40·9	191·6	164·7	221·1	233·1	262·6	227·0	420·9	295·0	247·5	470·5	299·1	256·8
Zr	17·4	13·8	10·3	6·2	18·1	24·5	14·6	12·9	18·3	17·4	7·7	35·6	10·5	19·4
Y	6·6	9·0	5·5	3·7	7·0	8·6	6·8	6·5	5·6	6·6	5·1	4·7	0·9	8·7
Nb	0·8	0·0	0·0	0·0	0·5	0·3	0·0	0·0	0·2	0·8	0·5	0·4	0·9	1·8
Ga	4·7	5·5	12·3	11·7	13·4	13·9	16·4	14·0	22·7	22·8	18·1	24·6	16·0	19·5
Cu	14·9	17·8	14·7	12·1	17·6	34·9	20·1	92·0	28·8	311·5	444·9	2·9	6·3	185·4
Zn	113·6	82·4	50·0	64·7	43·8	48·3	38·0	53·4	29·4	87·4	91·6	32·1	134·6	91·1
Mode %														
Plag	6	9	45	37	54	56	61	49	85	58	49	84	53	51
Opx	78	54	31	49	21	22	16	23	0	0	0	0	0	0
Cpx	16	36	22	13	25	21	22	26	6	16	19	1	3	24
Pig	0	0	0	0	0	0	0	0	8	14	19	6	0	0
Ol	0	0	0	0	0	0	0	0	0	0	0	0	36	17
Mt	0	0	0	0	0	0	0	0	0	8	9	4	3	5
Ilm	0	0	0	0	0	0	0	0	0	2	1	2	2	3
Ap	0	0	0	0	0	0	0	0	0	0	0	0	0	0
Qtz	0	0	0	0	0	0	0	0	0	0	0	0	0	0
Kspar	0	0	0	0	0	0	0	0	0	0	0	0	0	0
Residual[3]	0·57	0·31	0·23	0·66	0·42	1·4	1·3	0·36	1·1	0·74	0·28	2·5	0·52	2

(continued)

Table 1: Continued

Sample no.:	B06-054	B06-042	B06-039	B06-029	B07-026	B07-027	B07-028	B06-037	B06-056	B07-036	B07-037	B07-038	B07-040	B07-041
Height (m):[1]	3634	3741	3925	4083	4154	4232	4255	4305	4438	4460	4508	4530	4555	4590
Lithology:[2]	mt an	mt gb	mt gb	ol–mt gb	ol–mt gb	ol–mt gb	an	ol–mt gb	ol–mt gb	ol–mt gb	ol–mt gb	ol–mt gb	ol–mt gb	ol–mt gb
Oxide wt %														
SiO_2	50·12	44·97	45·10	39·14	46·44	40·69	47·25	41·94	38·37	44·61	45·88	49·51	46·07	47·00
TiO_2	1·27	2·56	3·06	2·89	3·16	2·88	3·07	2·80	3·57	2·67	2·51	1·77	2·49	2·16
Al_2O_3	22·98	13·34	13·53	13·45	17·11	15·57	21·36	15·99	11·36	13·53	14·82	12·86	14·58	12·68
FeO*	8·07	17·28	18·03	21·76	14·78	20·70	13·09	20·29	27·20	21·03	19·27	20·24	19·95	20·75
MnO	0·08	0·20	0·23	0·24	0·16	0·22	0·10	0·21	0·36	0·31	0·28	0·39	0·31	0·35
MgO	1·39	6·05	5·06	5·04	3·18	4·33	0·74	4·47	3·82	3·08	2·49	1·15	2·50	1·93
CaO	10·31	10·60	10·72	9·72	10·54	9·06	8·30	8·92	8·50	8·81	8·50	8·21	8·58	8·51
Na_2O	4·03	2·28	2·46	2·61	3·27	3·06	4·18	3·14	2·30	2·88	3·14	3·03	3·03	2·93
K_2O	0·51	0·36	0·27	0·25	0·32	0·31	0·58	0·32	0·54	0·58	0·90	1·04	0·81	0·82
P_2O_5	0·02	0·08	0·03	2·35	0·04	1·86	0·18	1·60	2·13	1·39	1·15	0·58	1·06	0·82
Sum	98·77	97·72	98·49	97·45	98·99	98·65	98·85	99·69	98·15	98·88	98·95	98·80	99·37	97·96
ppm														
Ni	9·6	30·5	43·4	0·0	11·0	28·8	17·3	17·2	0·8	2·0	0·9	0·8	0·8	0·0
Cr	5·3	0·0	8·2	1·7	14·1	8·7	115·7	8·3	4·6	4·4	3·0	1·4	4·6	0·1
Sc	15·5	52·4	58·4	21·3	50·4	16·1	11·2	17·1	26·2	35·8	34·1	73·1	35·8	68·8
V	183·4	479·6	423·1	60·8	69·4	43·5	135·2	41·2	32·0	14·9	4·8	3·6	2·5	1·7
Ba	189·5	130·9	126·4	106·4	124·6	110·5	266·8	113·3	204·4	211·1	402·2	414·6	355·4	321·9
Rb	9·7	7·8	4·2	1·4	3·7	2·5	8·1	4·2	13·9	13·6	21·3	33·2	21·6	22·3
Sr	424·9	216·9	249·9	254·2	355·4	315·7	433·1	320·8	258·3	299·5	328·6	280·1	329·1	277·4
Zr	20·2	27·0	21·8	5·9	9·6	12·6	40·3	12·7	55·6	75·9	85·9	99·7	86·0	103·0
Y	7·9	9·7	9·5	17·1	4·3	10·8	8·3	10·9	37·0	32·5	34·2	30·5	34·7	32·9
Nb	1·1	0·6	0·6	0·7	0·7	1·3	2·8	0·7	5·7	5·5	5·6	6·6	6·4	5·6
Ga	24·0	16·9	18·6	16·7	21·0	20·2	27·6	18·8	17·9	18·8	21·1	21·0	21·3	19·4
Cu	133·2	288·1	108·0	115·8	5·0	87·9	16·8	78·1	59·4	49·7	42·2	35·6	38·8	40·2
Zn	57·5	104·1	118·8	114·8	90·3	112·3	95·7	104·8	205·8	181·1	165·1	178·0	182·0	182·0
Mode %														
Plag	79	44	46	46	59	54	76	55	37	46	48	40	49	42
Opx	0	0	0	0	0	0	0	0	0	0	0	0	0	0
Cpx	9	29	30	10	23	5	5	6	12	16	15	17	16	20
Pig	0	0	0	0	0	0	0	0	0	0	0	0	0	0
Ol	5	17	12	24	3	23	6	22	27	24	21	4	20	19
Mt	4	3	6	7	9	7	8	7	8	0	0	17	0	2
Ilm	2	4	4	4	4	4	4	4	5	5	5	0	5	4
Ap	0	0	0	6	0	5	0	4	5	3	2	2	2	2
Qtz	0	0	0	0	0	0	0	0	0	1	0	14	0	4
Kspar	0	0	0	0	0	0	0	0	4	4	7	6	5	5
Residual[3]	2·2	0·76	0·93	0·65	0·42	0·93	1·9	0·58	0·75	1·1	1	1·2	2·3	0·03

*Total Fe given as FeO.
[1]Height is given in metres above the Merensky Reef.
[2]Lithological abbreviations: px, pyroxenite; gb, gabbro; an, anorthosite; tr, troctolite; di, diorite; mt-, magnetite-bearing; ol-, olivine-bearing.
[3]Sum of the squares of the residuals from the least-squares analysis.

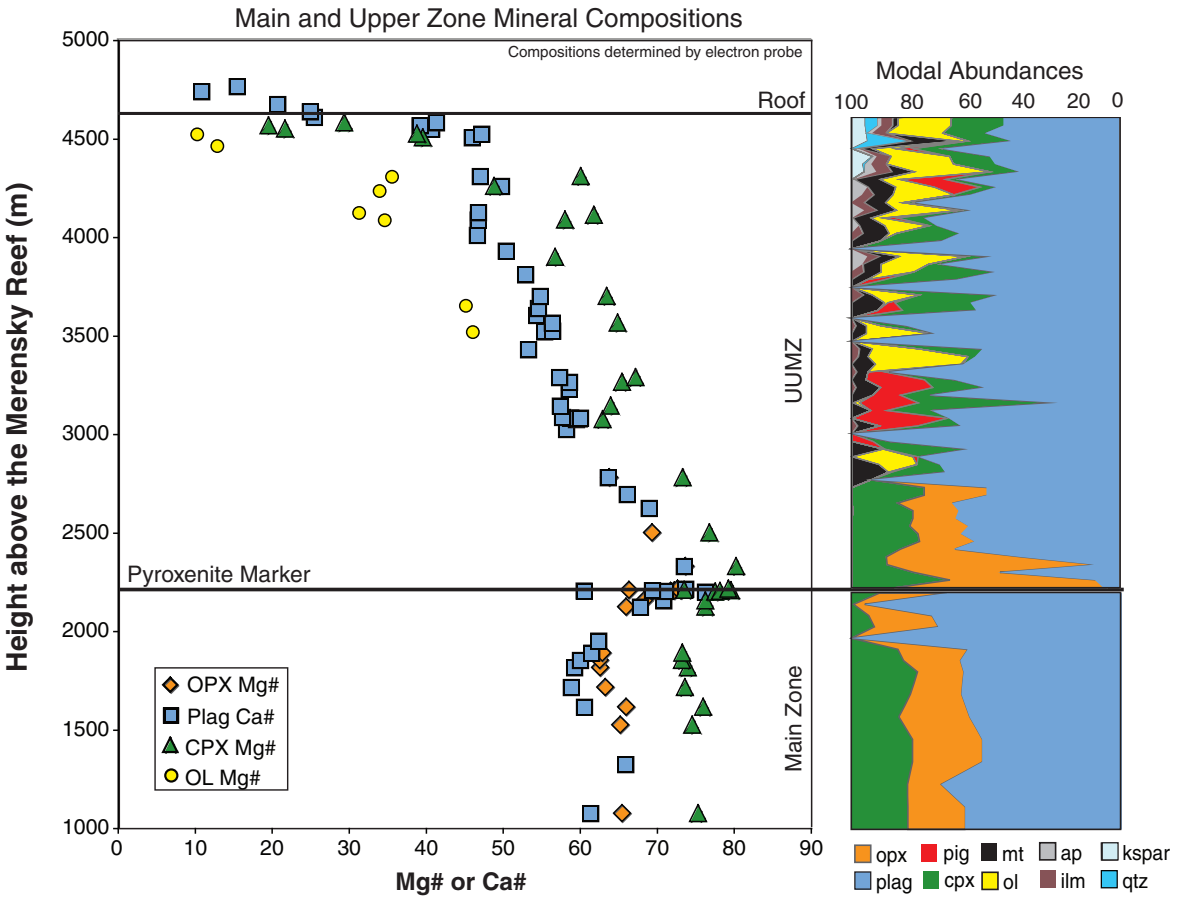

Fig. 4. Compositions of clinopyroxene (CPX), orthopyroxene (OPX), plagioclase (PLAG), and olivine (OL) throughout the UUMZ stratigraphy. Inverted pigeonite replaces orthopyroxene at 2830 m and is not included here because its original Mg-number cannot be directly determined. Mg-number calculated as molar $Mg/(Mg + Fe_{tot})$ and Ca-number calculated as molar $Ca/(Ca + Na)$. Height is in meters above the Merensky Reef. The Pyroxenite Marker in the eastern Bushveld is at 2200 m, and the roof of the UUMZ is at 4625 m. Modes are calculated via least squares from bulk-rock analyses and mineral compositions and verified optically in thin section (see text for details).

is located *c.* 1·5 km stratigraphically above the base of the UUMZ, corresponding to a pressure difference between it and the start of crystallization of *c.* 50 MPa. Thus, an initial pressure of 200 MPa was used in all MELTS runs.

The UUMZ gabbros themselves provide two constraints on the H_2O content of the magma. First, the apatite present in the upper third of the Upper Zone is essentially fluorapatite with only a low hydroxyl-apatite component (Boudreau *et al.*, 1986). Second, hydrous phases such as biotite and hornblende are restricted to interstitial assemblages but are absent as cumulus phases throughout the sequence, implying that the water contents of the main magma body never reached levels at which these phases would have become stable. Both observations suggest that water was a minor component of the magma. Thus, an initial H_2O content of 1 wt % is included in all of the model runs, which is also in accord with the average concentration in bulk-rock analyses reported by Bowes *et al.* (1997). Because H_2O is incompatible, however, it builds up in the MELTS runs as fractional crystallization proceeds, and eventually biotite becomes stable. Therefore, biotite crystallization is artificially suppressed in the MELTS runs. This probably has the effect of enhancing the abundances of both orthoclase and fayalitic olivine near the top of the crystallization sequence. The MELTS runs suggest that the UUMZ may have remained open to H_2O and oxygen during crystallization. The effects of varying pressure, fO_2 and H_2O content on the crystallization of orthopyroxene in the MELTS runs are explored in Supplementary Data Table 1 (available for downloading at http://www.petrology.oxfordjournals.org).

RESULTS

The bulk composition of the UUMZ

The UUMZ major element bulk composition was determined by combining 34 published bulk-rock analyses (Bowes *et al.*, 1997) of samples from the Magnet Heights

section of Molyneux (1974) with the new bulk-rock analyses from that same section reported here (Table 1). All samples and their stratigraphic weights used in the calculation of the bulk composition are provided in Supplementary Data Table 2. The new samples were selected based on their lithological representativeness of the stratigraphic interval in which they were found. Analyzed samples are spaced 10–50 m apart throughout the section. To generate a bulk composition of the UUMZ, single analyses were weighted and summed according to the stratigraphic interval that they represent. The bulk UUMZ trace element composition was determined using only the new analyses presented in Table 1.

According to Molyneux (1974), nearly monomineralic anorthosite accounts for *c.* 3% of the stratigraphic section above the Pyroxenite Marker. Compositions of the anorthosite layers were determined from a total of nine bulk-rock analyses. These analyses were then weighted to the thickness of the anorthosite layers they represent according to the stratigraphic column of Molyneux (1974).

Nearly monomineralic magnetitite layers account for *c.* 1% of the Upper Zone stratigraphy (Molyneux, 1974). To establish their compositions, we determined the composition and proportion of magnetite and ilmenite in each magnetitite layer via electron microprobe. Collectively they are estimated to be composed of 85% titanomagnetite + 15% ilmenite based on petrographic examination, whereas the Main Magnetite Layer is estimated to be composed of 100% titanomagnetite ($Usp_{39}Mt_{61}$ from electron microprobe analysis). Vanadium (ppm) and Cr (ppm) data on magnetitite layers in the eastern Bushveld were taken from Reynolds (1985). Each sample analyzed was then weighted for the magnetitite layer thickness it represents and added back to the bulk composition. Imprecisions in these estimates do not significantly influence the calculated bulk composition.

The calculated bulk composition of the UUMZ is presented in Table 2. By employing a jack-knife statistical re-sampling technique we are able to show that the UUMZ bulk composition calculated here is highly robust and is unlikely to change with additional sampling (see Supplementary Data Table 3 and discussion therein). In addition to providing trace elements, this composition is improved over that of Tegner *et al.* (2006) for two reasons. First, of the 33 bulk-rock compositions reported by von Gruenewaldt (1971) from the Magnet Heights section of Molyneux (1970) and used by Tegner *et al.* (2006) in their average, six are anorthositic. This translates to roughly 18% of the total, but anorthosite layers constitute only 3% of the total stratigraphy. Second, Tegner *et al.* (2006) averaged the analyses to generate bulk compositions of the subzones of the UUMZ and then generated a bulk composition by weighting the subzone compositions by their stratigraphic thicknesses. By doing this, closely spaced samples (e.g. 5–10 m apart) within a subzone were given the same weight as samples representing far larger proportions of the cumulate sequence (e.g. >100 m apart), resulting in a bulk composition not only biased towards that of the densely sampled sections of the stratigraphy, but also potentially biased towards the subzones with the largest total thickness regardless of sampling density. This approach yielded a bulk composition with significantly different FeO (>2 wt %) and Al_2O_3 (~1 wt %) contents from that reported here.

Observed and calculated modes

The modal abundances of all major phases were calculated for each sample by least squares (Bryan *et al.*, 1969) using the bulk-rock analyses and major-element mineral compositions determined by electron microprobe (Table 1; Fig. 4). The derivation of modal abundance from bulk composition will inevitably fail to account for pigeonite because it has inverted to orthopyroxene containing clinopyroxene lamellae. In pigeonite-bearing rocks (those above 2830 m in the stratigraphic column) all of the orthopyroxene calculated by the least-squares method is reported as primary pigeonite. Although this method results in a small bias towards the Ca-bearing phases (i.e. clinopyroxene and plagioclase) in the least-squares analysis, the resulting values are within a few per cent of the true values. In the figures and discussion that follow, the assumption is that these modes reflect true cumulus modes, as opposed to total-rock mode. This assumption was verified by the petrographic observation that equant (i.e. cumulus) phases far dominate the modes in all single samples. The calculated modal percentages were also confirmed by visual inspection in thin section.

To simulate fractional crystallization, MELTS calculates the composition and mass of each phase at each temperature step and subtracts them from those of the bulk liquid to generate both a new liquid composition and mass. To obtain the 'rock mode' at each temperature step the phase proportions (in volume) are summed and set to one, and the percentage of each phase is calculated. The per cent liquid remaining (y-axis, Fig. 5) was converted to a stratigraphic depth assuming either no magma loss (i.e. Fig. 5b, where 1% corresponds to 24·25 m because the total depth of the extant rock column is equal to 2425 m), or 15% magma loss (i.e. Fig. 5d–g, where 1% corresponds to 28·5 m because the original magma chamber would be 2425 m = 0·85X; X = 2852 m). The calculation of modes in this manner obviously does not take into account crystal settling or other dynamic magma chamber processes, which affect the observed rocks but not the liquid line of descent.

MELTS major element modeling

As noted, the estimated parent magma composition of the UUMZ must (1) initially crystallize the assemblage

Table 2: Bulk UUMZ composition and parent magma compositions used in the MELTS modeling

	1 Bulk UUMZ composition	2 Damwal Formation	3 Kwaggasnek Formation	4 Schrikkloof Formation	5 Rashoop Granophyre	6 15% Damwal: 85% UUMZ	7 15% Kwaggasnek: 85% UUMZ	8 15% Schrikkloof: 85% UUMZ	9 15% Rashoop: 85% UUMZ	10 25% Damwal: 75% UUMZ	11 25% Kwaggasnek: 75% UUMZ	12 25% Schrikkloof: 75% UUMZ	13 25% Rashoop: 75% UUMZ	14 Tegner *et al.* (2006) proposed parent magma
SiO_2	47·03	68·30	72·30	74·40	73·91	50·22	50·82	51·14	51·06	52·35	53·35	53·87	53·75	51·40
TiO_2	1·74	0·60	0·35	0·24	0·25	1·56	1·53	1·51	1·51	1·45	1·39	1·36	1·36	1·00
Al_2O_3	16·37	12·20	11·60	11·60	11·97	15·75	15·66	15·66	15·71	15·33	15·18	15·18	15·27	16·60
FeO*	15·60	7·18	5·24	3·20	3·45	14·34	14·05	13·74	13·78	13·50	13·01	12·50	12·56	11·70
MnO	0·20	0·14	0·14	0·03	0·08	0·19	0·19	0·18	0·19	0·19	0·19	0·16	0·17	0·10
MgO	6·48	1·09	0·66	0·61	0·53	5·67	5·60	5·60	5·58	5·13	5·02	5·01	4·99	4·60
CaO	9·39	2·31	0·69	0·24	0·3	8·32	8·08	8·01	8·02	7·62	7·21	7·10	7·11	9·70
Na_2O	2·46	2·84	2·69	2·62	3·12	2·51	2·49	2·48	2·56	2·55	2·51	2·50	2·62	2·90
K_2O	0·36	4·17	5·07	5·82	5·48	0·93	1·06	1·18	1·13	1·31	1·54	1·72	1·64	0·70
P_2O_5	0·38	0·15	0·05	0·02	0·03	0·34	0·33	0·32	0·33	0·32	0·30	0·29	0·29	0·40
Sum	100·00	100·10	100·30	100·00	99·12	100·02	100·05	100·00	99·87	100·03	100·08	100·00	99·78	99·10
molar Fe/Mg	1·35	3·70	4·45	2·94	3·65	1·42	1·41	1·38	1·38	1·48	1·45	1·40	1·41	1·43
molar Ca/Na	8·45	1·80	0·57	0·20	0·21	7·32	7·17	7·14	6·94	6·60	6·34	6·29	6·00	7·39
ppm														
Ni	84	6	4	1	0	73	72	72	72	65	64	63	63	–
Cr	92	8	5	2	3	79	79	78	78	71	70	69	70	–
Sc	35	13	7	1	3	32	31	30	30	30	28	27	27	–
V	315	3	0	0	0	269	268	268	268	237	237	237	237	–
Ba	117	862	1012	1349	846	229	251	302	227	303	341	425	299	–
Rb	5	163	215	232	289	29	37	39	48	45	58	62	76	–
Sr	260	145	101	34	82	243	236	226	233	231	220	203	215	–
Zr	22	376	475	601	628	75	90	108	113	110	135	166	173	–
Y	10	56	69	81	109	17	19	21	25	22	25	28	35	–
Nb	1	18	23	30	38	4	4	5	7	5	7	8	10	–
Ga	17	17	17	18	20	17	17	17	18	17	17	18	18	–
Cu	132	38	13	4	0	118	114	112	112	108	102	100	99	–
Zn	94	150	152	46	188	102	102	86	108	108	108	82	117	–

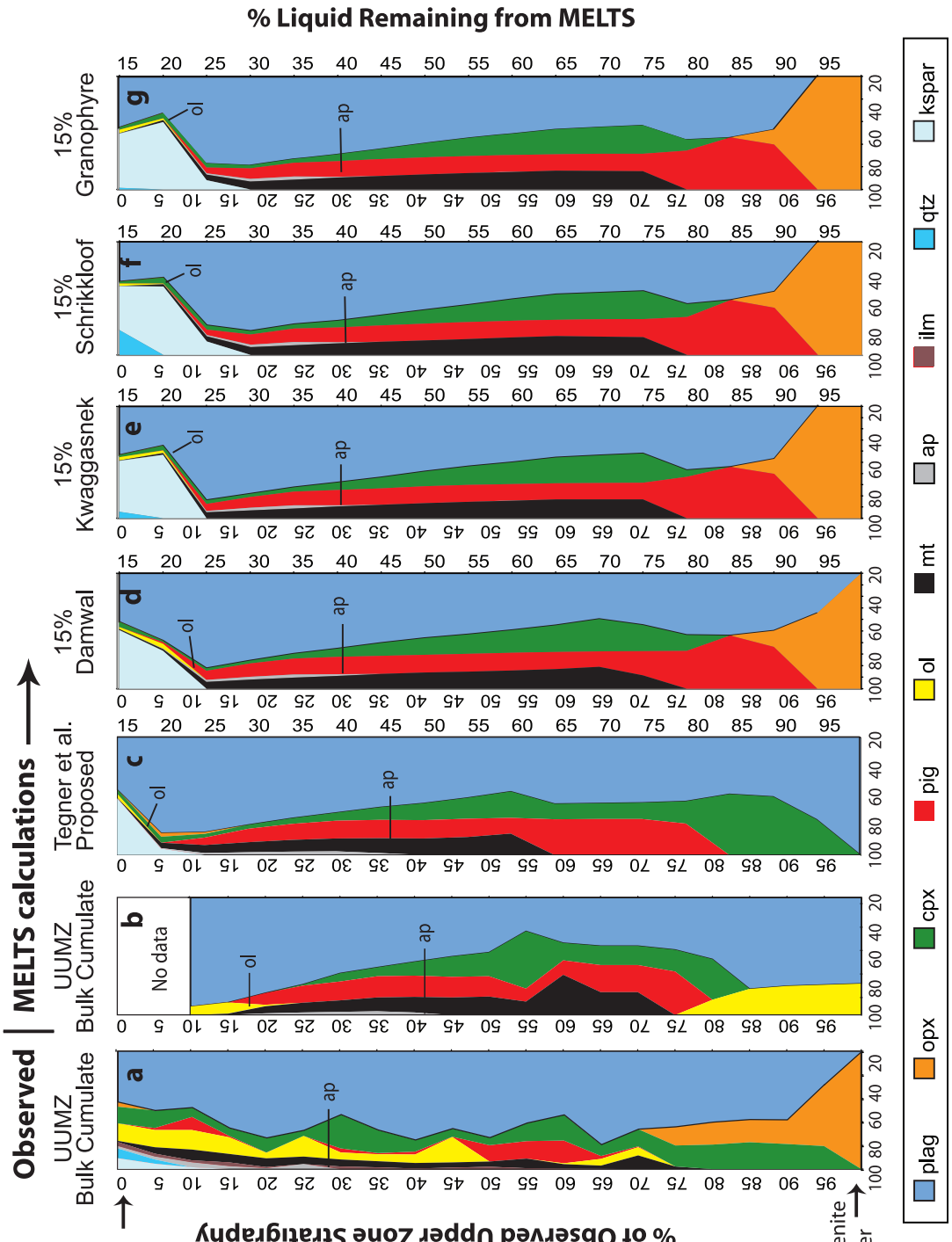

Fig. 5. Observed variation in modal abundance through the UUMZ compared with the modal abundances predicted by MELTS. All runs were conducted at $P = 200$ MPa, $fO_2 = \text{FMQ}$ and 1 wt % H_2O. The left *y*-axis is the per cent of the rock column remaining, where 100% is the base of the UUMZ and 0% is the contact with the roof. The right *y*-axis is the per cent liquid remaining from the parent magma. For accurate comparison with the observed modes, MELTS outputs are shown in volume per cent. (a) Observed modal stratigraphy of the Magnet Heights section for the UUMZ cumulates. The modal variations are smoothed from Fig. 4 for easier comparison with MELTS results. In some cases, especially near the base, it is difficult to determine whether some clinopyroxene grains are cumulus or interstitial; in these cases, the total rock mode is assumed to represent the cumulus mode. (b–g) The predicted modal stratigraphies from MELTS experiments for (b) bulk UUMZ composition; (c) UUMZ parent magma composition of Tegner *et al.* (2006); (d) bulk UUMZ + 15% Damwal lava; (e) bulk UUMZ + 15% Kwaggasnek lava; (f) bulk UUMZ + 15% Schrikkloof lava; (g) bulk UUMZ + 15% Rashoop Granophyre. Mineral abbreviations are as in Fig. 4, and pig, pigeonite; mt, magnetite; ap, apatite; ilm, ilmenite; qtz, quartz; kspar, orthoclase. The fields of olivine and apatite should be noted; both of these are labeled to highlight the level of their appearance. The parent magma compositions used in the MELTS experiments are shown in Table 2. Parent magmas in which 15–25% Rooiberg lava or Rashoop Granophyre is added to the bulk UUMZ composition crystallize orthopyroxene at the base and generally crystallize the observed paragenetic sequence.

orthopyroxene and the other observed cumulus phases at the base of the section, (2) crystallize minerals of the observed compositions, and (3) generally reproduce the observed paragenetic sequence.

Crystallization of orthopyroxene at the base: MELTS modeling results

The MELTS results for the bulk UUMZ composition + 1 wt % H_2O show that this composition does not satisfy the first-order constraint of initial orthopyroxene crystallization (Fig. 5b). Thus, consistent with the conclusion of Cawthorn & Walraven (1998), the existing cumulate sequence does not constitute the bulk liquid from which it formed, and some amount of magma must have escaped. The parent magma composition of Tegner *et al.* (2006), in which a liquid in equilibrium with most UUMZ phases was added to their bulk composition, also does not crystallize orthopyroxene at the base (Fig. 5c).

MELTS results of the UUMZ bulk cumulate plus the overlying Rooiberg Group lava units are presented in Fig. 5d–f. The Rooiberg lava compositions used to generate the parent magma compositions are from Schweitzer *et al.* (1997) and are provided in Table 2. These were chosen because of the distinction between Kwaggasnek and Schrikkloof lava compositions, whereas Buchanan *et al.* (2002) provided analyses of the Dullstroom, Damwal and Kwaggasnek, but not the Schrikkloof lavas. Regardless, both sets of data yield similar results in the MELTS runs (Supplementary Fig. 1). Each of the Rooiberg units was added back to the bulk composition in increments of 5% until a composition initially saturated in orthopyroxene was found. This constraint was satisfied by parent magmas in which a minimum of 15% and a maximum of 25% Damwal, Kwaggasnek, or Schrikkloof lava were added to the bulk UUMZ composition (Table 2). Because of the similarity in composition between the Rooiberg lavas and the Rashoop granophyres, we also investigated a parent magma in which the latter represents the expelled melt. Not surprisingly, this parent magma also crystallizes orthopyroxene as the primary phase with 15–25% granophyre addition (Fig. 5g).

With two exceptions, all bulk compositions in the MELTS runs that initially crystallize orthopyroxene also generally reproduce the paragenetic sequence inferred from the observed stratigraphic sequence. For example, titanomagnetite enters as a cumulus phase in the MELTS runs after *c.* 25% crystallization (Fig. 5d–f), similar to what is seen in the UUMZ, and apatite enters after c. 70% crystallization, also identical to the observed UUMZ stratigraphy.

One exception is the significantly delayed appearance of fayalitic olivine. As discussed above, this is probably due to the parameterization of fO_2 in the MELTS simulations. A second discrepancy concerns the nature of the pyroxenes at the base of the section. In the MELTS simulations clinopyroxene appears somewhat later than in the actual rock column and pigeonite replaces orthopyroxene at about the point when clinopyroxene becomes stable (Fig. 5). It can be seen, however, that the observed UUMZ rocks suggest the paragenetic sequence opx → opx + plag + cpx → pig + plag + cpx. This discrepancy results from the fact that the difference in Gibbs free energy among the competing pyroxenes is very small. Thus, because MELTS is calibrated as a Gibbs free energy minimization algorithm, the discrepancy almost surely reflects a problem with the MELTS calibration. This problem should only arise, however, when there is more than one pyroxene at or near the liquidus (i.e. the choice of the second pyroxene phase, pigeonite or clinopyroxene, after orthopyroxene) and does not affect MELTS's ability to identify the composition of the first phase on the liquidus. Thus, we are confident in the use of MELTS to identify a parent magma with orthopyroxene as the initial crystallizing phase. As an aside, the late appearance of clinopyroxene in our MELTS simulations may have an additional cause that cannot be ruled out. Putirka *et al.* (1996, 2003) have shown that MELTS does not perfectly reproduce the appearance of clinopyroxene when given experimental melt compositions with clinopyroxene on the liquidus.

Mineral compositions: agreement with MELTS output

The mineral compositions predicted by the MELTS runs deviate slightly from the actual observed compositions. In particular, the composition of orthopyroxene at the base of the column is $En_{70}Fs_{27}Wo_3$, whereas the first orthopyroxene to crystallize in the MELTS runs is approximately $En_{73}Fs_{23}Wo_4$. For plagioclase, those just above the Pyroxenite Marker have a composition of $An_{73}Ab_{26}Or_1$, whereas MELTS returns a composition of $An_{75}Ab_{24}Or_1$. These slight discrepancies may be because MELTS overestimates liquidus temperature (e.g. Hirschmann *et al.*, 1998). In the case of orthopyroxene, an alternative is that the observed composition may have been modified by sub-solidus re-equilibration with clinopyroxene. Consistent with this is the fact that observed clinopyroxene compositions also display proportionally higher En–Wo than predicted by MELTS ($En_{44}Fs_{11}Wo_{45}$ in the UUMZ vs $En_{43}Fs_{17}Wo_{40}$ in all of the MELTS runs). Regardless of these slight discrepancies, MELTS predicts mineral compositions nearly identical to the observed UUMZ for all runs in which orthopyroxene is the primary phase.

Major element crystal–liquid equilibrium compositions

As an independent test of the MELTS results, we use the measured mineral compositions at the base of the UUMZ to determine an equilibrium liquid composition. While some sub-solidus re-equilibration is likely to have affected the observed mineral compositions, particularly pyroxene

Fe/Mg, taken as a whole they still provide useful constraints on the composition of the equilibrium liquid.

The Fe/Mg of the equilibrium liquid can be calculated from orthopyroxene using

$$K_d \frac{(Fe^{opx}/Mg^{opx})}{(Fe^{liq}/Mg^{liq})} = 0{\cdot}2 - 0{\cdot}3 \quad \text{(Bedard, 2007)}$$

Bedard (2007) estimated the Fe–Mg exchange for orthopyroxene–melt to be between 0·2 and 0·3, with melts having MgO > 12 wt % displaying near-constant $K_d = 0{\cdot}3$. For melts with MgO < 12 wt %, the K_d decreases gradually from 0·3 to 0·2. The MgO content of the liquid in equilibrium with the base of the UUMZ is likely to have been between 5 and 7 wt %, equivalent to a K_d between 0·24 and 0·27. For the purpose of this study, we choose a K_d Fe–Mg of 0·25 for orthopyroxene–liquid, similar to that identified by Baker & Eggler (1987) for anhydrous basalt.

Estimates of Fe/Mg_{liq} from orthopyroxene at the base of the UUMZ are within the range of the proposed parent magmas (Table 3). The effect of sub-solidus re-equilibration will be for orthopyroxene to gain Fe from clinopyroxene, thus increasing Fe/Mg_{opx} and predicted Fe/Mg_{liq} (Saxena *et al.*, 1986). The effects of these re-equilibrations will be greatest on the less abundant phase. Orthopyroxene is approximately 2–4 times more abundant than clinopyroxene in the gabbros directly above the Pyroxenite Marker, so sub-solidus re-equilibration will have relatively little effect on its composition. At the base of the UUMZ, the predicted equilibrium Fe/Mg_{liq} from orthopyroxene is consistent with the proposed parent magma compositions calculated by adding 15–25% Rooiberg lavas to the UUMZ composition, but is inconsistent with the hypothesis that the UUMZ crystallized as a closed system (Table 3).

Plagioclase is the dominant phase throughout the entire UUMZ and in many cases it makes up more than 50% of the mode. Unlike the pyroxenes, however, plagioclase has the added benefit of being relatively unsusceptible to sub-solidus re-equilibration. The Ca/Na content of the equilibrium liquid can be calculated from plagioclase using

$$\frac{(Ca^{plag}/Na^{plag})}{(Ca^{liq}/Na^{liq})} = 1{\cdot}56 \text{ (Aigner-Torres } \textit{et al.}\text{, 2007)}$$

The plagioclase Ca–Na K_d can vary substantially because of its large dependences on temperature and aH_2O. A recent experimental estimate of $D_{Ca} = 1{\cdot}26$, and an estimate of $D_{Na} = 0{\cdot}806$ in a natural MORB sample (Aigner-Torres *et al.*, 2007), can be used to calculate an approximate K_d of 1·56. Using this estimate, the calculated Ca/Na equilibrium liquid from plagioclase at the base of the UUMZ agrees well with the Ca/Na of the proposed parent magmas of this study in which 15–25% Rooiberg

Table 3: Fe/Mg and Ca/Na equilibrium liquid compositions from orthopyroxene and plagioclase at the base of the UUMZ

	Orthopyroxene				
Sample no.:	B06-061	B06-060	B07-007	B07-009	B06-062
Height (m):	2199	2200	2203	2210	2325
Lithology:	gabbro	pyroxenite	pyroxenite	gabbro	gabbro
SiO_2	54·16	53·94	54·35	54·32	54·65
TiO_2	0·24	0·21	0·21	0·20	0·20
Al_2O_3	0·91	0·88	0·96	0·86	0·86
FeO	17·82	17·54	17·18	17·50	16·91
MgO	25·46	25·70	26·33	26·20	26·63
MnO	0·38	0·39	0·38	0·43	0·38
CaO	1·84	1·50	1·45	1·36	1·25
Na_2O	0·03	0·03	0·01	0·01	0·02
Cr_2O_3	0·12	0·12	0·14	0·13	0·10
Total	100·95	100·29	101·01	101·01	101·00
Molar Fe/Mg	0·39	0·38	0·37	0·37	0·36
Calculated Fe/Mg equilibrium liquid	1·57	1·53	1·46	1·50	1·42

	Plagioclase				
Sample no.:	B06-061	B06-060	B07-007	B07-009	B06-062
Height (m):	2199	2200	2203	2210	2325
Lithology:	gabbro	pyroxenite no cumulus plagioclase	pyroxenite no cumulus plagioclase	gabbro	gabbro
SiO_2	50·51			50·46	49·87
TiO_2	0·02			0·02	0·02
Al_2O_3	32·12			31·81	32·69
FeO	0·40			0·35	0·30
MgO	0·02			0·02	0·02
MnO	0·02			0·01	0·02
CaO	14·43			14·80	14·99
Na_2O	3·24			2·91	2·99
K_2O	0·21			0·21	0·19
Total	100·98			100·66	101·08
Molar Ca/Na	9·85			11·23	11·10
Calculated Ca/Na equilibrium liquid	6·31			7·20	7·12

	Proposed parent magma compositions		
	Range of 15% addition	Range of 25% addition	Bulk UUMZ composition
Fe/Mg	1·38–1·42	1·40–1·48	1·35
Ca/Na	6·94–7·32	6·00–6·60	8·45

lavas are added, and is significantly different from the bulk UUMZ composition (Table 3).

Trace element crystal–liquid equilibrium compositions

The concentration ranges of a number of trace elements, notably Sr, Cr, Ni, Zn and Cu, in the proposed parent magmas and the bulk UUMZ composition are very similar (Table 4), and thus do not serve as suitable tests for our hypothesis. The trace elements Zr, Y, Ba, and Rb, however, are sufficiently different to warrant their use as a test for trace element equilibrium. Here we present crystal–liquid equilibria for these four elements compared with the proposed parent magmas. The full trace element datasets for orthopyroxene and plagioclase at the base of the UUMZ are available in Supplementary Data Tables 4 and 5.

Zr and Y in orthopyroxene

The choice of appropriate trace element partition coefficient depends on the major element composition of the phase. Dunn & Sen (1994) published a series of experiments on orthopyroxene partition coefficients (D values) for basaltic–andesitic magmas at 1 bar. They reported a D_{Zr} of 0·021 and D_Y of 0·19 for orthopyroxene in the range of $En_{67–75}Fs_{21–29}Wo_{3–4}$, as is found at the base of the UUMZ. Using these values and the measured orthopyroxene compositions, the equilibrium liquid at the base of the UUMZ contained between 145 and 215 ppm Zr and between 17 and 22 ppm Y (Table 4). Thus, for both Zr and Y the calculated concentrations in the equilibrium liquid overlap (or are slightly above in the case of Zr) those of the proposed parent magmas (74–173 ppm Zr; 17–35 ppm Y), but they are significantly greater than the 21 ppm Zr and 10 ppm Y of the bulk UUMZ (Fig. 6).

Ba and Rb in plagioclase.

Plagioclase trace element partition coefficients vary considerably with major element composition. The dependence of D_{Ba} and D_{Rb} varies with the mole fraction of anorthite (X_{An}) following

$RT \ln D_{Ba} = 10200 - 38200\ X_{An}$ (Blundy & Wood, 1991)
$RT \ln D_{Rb} = -40\ X_{An} - 15{\cdot}1$ (Bindeman *et al.*, 1998).

Using these equations and a constant $T = 1100°C$, the calculated equilibrium liquid at the base of the UUMZ contains *c.* 337 ppm Ba and between 31 and 34 ppm Rb (Table 4). These predicted values both fall within their respective ranges in the proposed parent magmas (228–425 ppm Ba, 29–76 ppm Rb), but again they are significantly greater than the UUMZ bulk composition of 117 ppm Ba and 5 ppm Rb (Fig. 6).

Table 4: In situ LA-ICPMS trace element mineral compositions and calculated equilibrium liquids

Zr and Y in orthopyroxene			
Sample no.:	B06-061	B06-060	B07-009
Height (m):	2199	2200	2210
Lithology:	gabbro	pyroxenite	gabbro
Mg-no.	71·80	72·31	72·74
n:	5	25	11
Average measured in situ *LA-ICPMS*			
Zr (ppm)	5·44 (0·50)	4·51 (0·81)	2·94 (0·39)
Y (ppm)	4·17 (0·25)	4·12 (0·53)	3·11 (0·17)
Calculated equilibrium liquid composition			
Zr (ppm)	259·0	214·8	140·0
Y (ppm)	21·9	21·7	16·4

Range of proposed parent magmas			
	Bulk UUMZ	15% addition	25% addition
Zr (ppm)	21·6	74–112	110–173
Y (ppm)	10	16·9–24·9	21·5–34·8

Ba and Rb in plagioclase			
Sample no.:	B06-061	B06-060	B07-009
Height (m):	2199	2200	2210
Lithology:	gabbro	pyroxenite	gabbro
An:	70·20		72·9
n:	14	all interstitial	10
Average measured in situ *LA-ICPMS*			
Ba (ppm)	90·35 (7·50)		75·31 (4·40)
Rb (ppm)	0·77 (0·13)		0·53 (0·07)
Calculated equilibrium liquid composition			
Ba (ppm)	387·8		352·8
Rb (ppm)	34·0		25·5

Range of proposed parent magmas			
	Bulk UUMZ	15% addition	25% addition
Ba (ppm)	117·2	226–302	299–425
Rb (ppm)	5·2	29–48	45–76

n, number of analyses in average. Values in parentheses are 1σ standard deviation.

DISCUSSION

Amount and composition of the expelled melt

Three lines of evidence provide the basis for the conclusion that the bulk UUMZ composition does not represent a

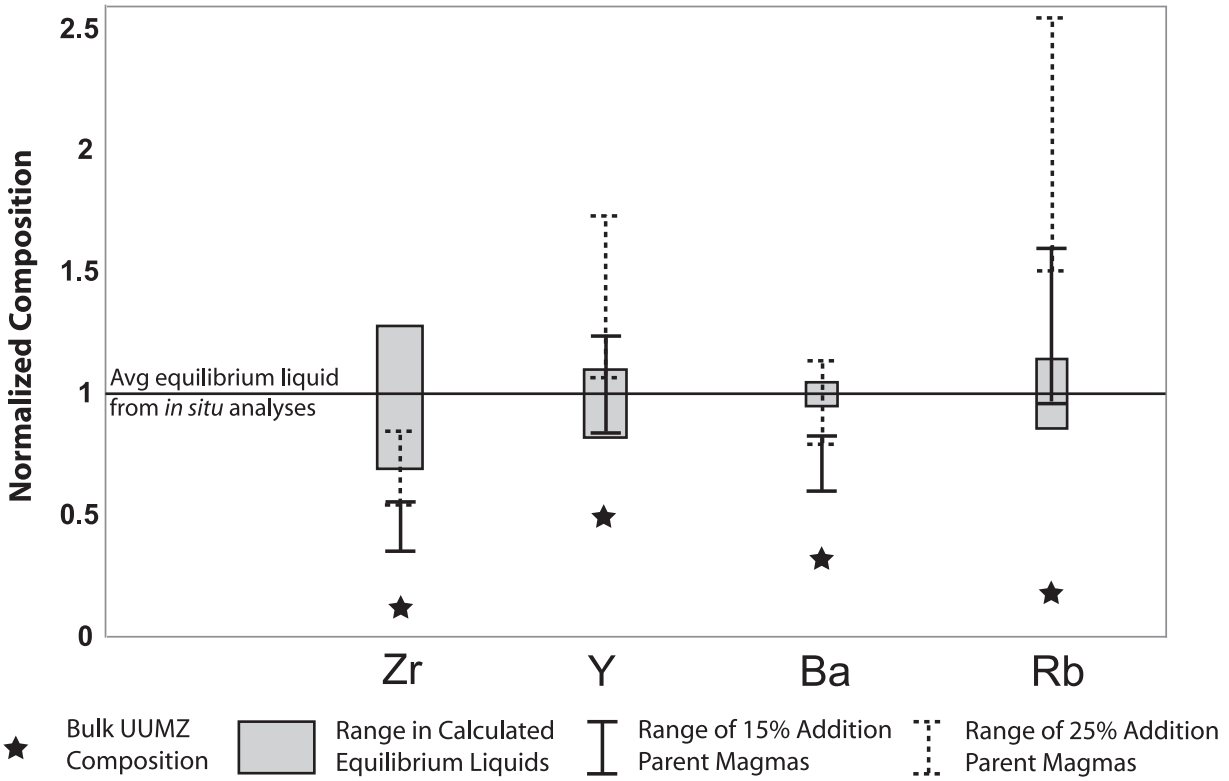

Fig. 6. Comparison of calculated trace element equilibrium liquid compositions from *in situ* analyses of orthopyroxene and plagioclase near the base of the UUMZ with the proposed UUMZ parent magma compositions. For plotting, all compositions (ppm) are normalized to the average equilibrium liquid composition calculated from the *in situ* mineral analyses (Zr and Y from orthopyroxene; Ba and Rb from plagioclase; Table 5). In all cases, the average equilibrium liquid composition overlaps those of the proposed parent magmas (dashed and solid bars) and is far greater than that of the bulk UUMZ composition (filled stars).

viable liquid composition, and thus some amount of magma must be missing. The first is the mass-balance calculations of Cawthorn & Walraven (1998) suggesting that there is not enough Zr and K in the cumulate rocks to account for the amount input into the system (a conclusion corroborated by bulk-rock trace element analyses from our section; Fig. 3). The second is the lack of orthopyroxene saturation in the MELTS runs using the bulk composition of the UUMZ alone (Fig. 5). The third is the clear discrepancy in trace element composition between the calculated equilibrium liquid at the base of the UUMZ and the UUMZ bulk composition (Fig. 6).

The proposed parent magmas in which Rooiberg Group lava or Rashoop Granophyre is added to the UUMZ bulk composition satisfy all three of the criteria for an original parent magma of the UUMZ. First, they produce primary orthopyroxene at the beginning of the crystallization sequence (Fig. 5). Second, the proposed parent magma compositions are consistent with estimates of both major and trace element equilibrium liquid compositions calculated from the observed mineral compositions (Tables 3 and 4; Fig. 6). Third, for each of the proposed parent magma compositions, MELTS is able to approximate the observed paragenetic sequence, with the exception of fayalitic olivine, via fractional crystallization (Fig. 5).

In addition to constraining the parent magma composition of the UUMZ, the MELTS results allow us to estimate the amount of magma lost from the chamber. Specifically, our results suggest that between 15 and 25% of the original UUMZ magma chamber was expelled (Fig. 5). As a result of the highly evolved compositions of the Rooiberg lavas and Rashoop Granophyre, this most probably occurred late in the crystallization sequence after significant fractional crystallization had taken place.

Geological considerations

The translation of this percentage into an absolute volume of escaped liquid is complicated by limited knowledge of the original extent and connectivity of the Bushveld Complex. Considering the Rooiberg first, the simplest assumption is that the thickness of the lava suite should be in proportion to the amount of magma expelled from the UUMZ chamber. Twist (1985) estimated that the Rooiberg lavas in the area of Loskop Dam are 3560 m thick and gradually thicken to 5110 m to the east [as

Table 5: Lava thicknesses and equivalent percentage lost from the original UUMZ magma chamber

Expelled melt composition	Damwal Formation	Kwaggasnek Formation	Schrikkloof Formation	Kwaggasnek + Schrikkloof	All Upper Rooiberg
Observed lava thickness* (m)	1065	275	340	615	1680
Original UUMZ magma chamber (m)	3490	2700	2765	3040	4105
% expelled†	30·5	10·2	12·3	20·2	40·9

*The observed lava thickness comes from the stratigraphic column of Twist (1985) in the area of Loskop Dam in the eastern Bushveld. The unit numbers of Twist (1985) were further refined by Harmer & Farrow (1995) into Damwal, Kwaggasnek and Schrikkloof.
†Assuming the original spatial extent of the Rooiberg and the Bushveld was approximately equal. Because the Damwal Formation is found only in the eastern Bushveld, the translation of thickness into a percentage may not apply to that formation (see text for further description).

mapped by Clubley-Armstrong (1977)]. In the Loskop Dam area, the Damwal is by far the most voluminous formation with a thickness of 1065 m, whereas the Kwaggasnek and Schrikkloof formations average 275 m thick and 340 m thick, respectively (it should be noted that the remaining Rooiberg thickness consists of upper Dullstroom and interbedded sedimentary rocks). In the eastern Bushveld, the UUMZ is *c.* 2425 m thick. If the subaerial extent of the Rooiberg lavas and the UUMZ were roughly similar at the time of formation, then the proportional volumes can be calculated from the relative thicknesses of the units (Table 5). The Kwaggasnek and Schrikkloof lava thicknesses are well within the range predicted by this study. Although the Damwal percentage is too high (~30%), it should be noted that the Damwal is present only in the eastern Bushveld, and therefore its thickness may not be accurately equated with amount of magma expelled.

Quantification of the extent of the Rashoop Granophyre Suite is complicated by uncertainty in not only its stratigraphic distribution, but also its origin. Walraven (1985) suggested that the total thickness of the Rashoop Granophyre Suite can be in excess of 1000 m and argued that there are at least three distinct types of granophyre with different origins. According to Walraven (1985), the most voluminous is the Stavoren Granophyre, which has a geochemical signature nearly identical to that of the Kwaggasnek or Schrikkloof lavas, and probably formed as the intrusive equivalent to the lavas; the Diepkloof Granophyre, found only in the eastern Bushveld, is similar in composition to the Damwal Formation and was probably formed by remelting of Damwal lava in contact with the Bushveld magmas; and the Zwartbank Pseudogranophyre, which contains sedimentary xenoliths, probably formed by partial melting of Pretoria Group sediments. The lack of clear field relations and the compositional similarity with the Rooiberg lavas make it impossible to determine whether or not some or all of the Rashoop Granophyre represent melt expelled from the UUMZ.

Regardless of the role of the granophyre, a number of previously puzzling field observations become much more clear if the Bushveld magma chamber was the source of the Rooiberg lavas. First, eruptive centers have never been identified (Twist & French, 1983; Eriksson *et al.*, 1995). This is very unusual among large-volume silicic eruptions, which typically display clear evidence of caldera-forming events and extensive ash-flow tuffs (e.g. the Fish Canyon tuff). The absence of clear eruptive centers for the Rooiberg felsites suggests that the source of the lavas was effusive, perhaps occurring by fissure eruption from a number of shallow source chambers, in contrast to a conduit-fed eruption from a deep crustal source. Second, there are no sills or dikes of mafic material present anywhere in the Rooiberg Group lavas (J. Schweitzer, personal communication), as would be expected had the Bushveld intruded into the lava sequence.

Formation of the Rooiberg Group lavas

Such a large volume of anorogenic rhyolite as the Rooiberg Group must represent one of two processes: partial melting of continental crust, or differentiation of a large body of mafic magma (as proposed in this study). If the Rooiberg represents a partial melt of the continental crust mixed with a mafic, mantle-derived melt, (1) it should possess crustal isotopic signatures, which should vary depending on the mixing proportions of melted crust and mantle-derived mafic magma, and (2) its composition should be consistent with partial melting of a crustal source. Both of these criteria are examined below.

In all of the crustal melting scenarios proposed for the Rooiberg to date (Hatton & Schweitzer, 1995; Maier *et al.*, 2000), the proportion of the crustal component increases with increasing stratigraphic height from the Damwal to

the Schrikkloof. Yet, as Buchanan *et al.* (2004) pointed out, there is greater isotopic variability within than between each formation. The lack of systematic variation in isotopic composition is thus inconsistent with the idea of progressively increased crustal assimilation.

Additionally, the isotopic similarity between the dacitic–rhyolitic Rooiberg Group lavas and the ultramafic–mafic cumulates of the Bushveld Complex is inconsistent with the idea of crustal assimilation as the source of such highly radiogenic compositions. Presumably the mafic parent magmas of the Bushveld should have a greater proportion of mantle-derived (i.e. less radiogenic) magma than the felsic crustal-derived (i.e. more radiogenic) lavas of the Rooiberg Group. One possible explanation, however, is that crustal melting is not significant for either body. Richardson & Shirey (2008) showed that at least a portion of the subcontinental lithospheric mantle (SCLM) of the Kaapvaal craton below the Bushveld Complex is highly radiogenic in Sr, Nd, and Os isotopes. Thus, the isotopic characteristics of the Bushveld Complex may reflect a mantle source (that itself contains a crustal component) rather than requiring extensive crustal melting and assimilation of Kaapvaal crust. The same holds for the Rooiberg Group, if it were formed by fractionation of the SCLM-derived mafic melts.

Further evidence against a crustal-melt origin for the Rooiberg Group comes from major and trace elements. Buchanan *et al.* (2002) showed that the trends in major elements (particularly the decreasing amount of Al_2O_3) and trace elements (the increasing depletion in Sr, Sc, Co, Ni, P) with stratigraphic height in the upper Rooiberg Group lavas are not consistent with crustal assimilation. Instead, they demonstrated that the variations generally can be accounted for by fractional crystallization of plagioclase plus or minus augite, pigeonite, olivine, magnetite–ilmenite, and orthoclase, consistent with our results.

The alternative hypothesis suggested by our results, and supported by the data of Buchanan *et al.* (2002), is not new. Indeed, the notion of Bushveld differentiation to produce the Rooiberg Group (Daly & Molengraaff, 1924) or the Rashoop Granophyre (Lombaard, 1949) goes far back in Bushveld research. Perhaps now is the time to revisit these arguments in more detail.

CONCLUSIONS

In this study we have calculated a new bulk composition for the Bushveld Complex UUMZ, identified the major and trace element composition of the UUMZ parent magma, and developed constraints on the composition and quantity of magma lost from the Bushveld magma chamber. Our results show that the bulk composition of the UUMZ in the eastern Bushveld does not crystallize the observed mineral assemblage at the base of the crystallization sequence, and thus that some amount of evolved magma was expelled from the magma chamber during its crystallization. Results of MELTS runs show that the addition of 15–25% Rooiberg lava or Rashoop Granophyre to the UUMZ bulk composition will return a parent magma composition that is initially saturated in orthopyroxene and that reproduces generally the observed paragenetic sequence in the UUMZ.

Assuming that the UUMZ originally consisted of the residual liquids from the Lower, Critical and Main Zones plus an additional amount of new magma intruded at the Pyroxenite Marker, then the 15–25% of the original Upper Zone that escaped the magma chamber translates to *c.* 9% of the total original Bushveld magma chamber (assuming an 8 km thick extant Bushveld). This percentage is within the proposed range of the 5–10% total rhyolite produced by fractional crystallization of basaltic melt based on studies of Thingmuli and other Iceland volcanoes (Carmichael, 1964) (it should be noted that Thingmuli volcano itself is 21% rhyolite, 18% andesite, and 57% tholeiite and olivine tholeiite). Additionally, calculations of efficient fractional crystallization suggest that up to 12% felsic material can be generated from a tholeiitic and ~7% from an olivine tholeiitic parent magma (Carmichael, 1964). The proportions are likely to be greater for the SiO_2- and MgO-rich parent magmas proposed for the Bushveld Complex and other large layered intrusions, such as the Stillwater Complex (e.g. Irvine *et al.*, 1983; Harmer & Sharpe, 1985).

Perhaps the Bushveld Complex originated as a sub-volcanic magma chamber, as has been proposed for the Stillwater Intrusion of Montana (e.g. Helz, 1995). Alternatively, it is possible that the Bushveld Complex was initially a hypabyssal intrusion, where the overburden grew significantly thicker as erupted lava issued from the chamber late in the crystallization process and was deposited on the initially thin roof. Such a concept could account for both its planar character and enormous extent across the Transvaal basin.

Whatever its tectonic setting, the Bushveld Complex and associated Rooiberg Group lavas may play an important role in our future understanding of the possibility for, and the extent of, extreme igneous differentiation in shallow crustal magma chambers.

SUPPLEMENTARY DATA

Supplementary data for this paper are available at *Journal of Petrology* online.

ACKNOWLEDGEMENTS

The authors are greatly indebted to Tom Molyneux for his guidance in the field. J.A.V. would like to thank Louise Bolge for her patience and guidance in the laboratory work. The manuscript greatly benefited from conversations with Al Hofmann, Sarah Fowler,

Jim Webster, Charlie Mandeville, and Alexey Kaplan. We would also like to acknowledge the thorough reviews of L. Ashwal, C. Tegner, R. G. Cawthorn, and an anonymous reviewer. LDEO contribution #7378.

FUNDING

This work was supported by Geological Society of America Graduate Student Research Grant, and a Graduate Student Fellowship from the American Museum of Natural History, both awarded to J.A.V.

REFERENCES

Aigner-Torres, M., Blundy, J., Ulmer, P. & Pettke, T. (2007). Laser ablation ICPMS study of trace element partitioning between plagioclase and basaltic melts: an experimental approach. *Contributions to Mineralogy and Petrology* **153**, 647–667.

Ariskin, A. A., Frenkel, M. Y., Barmina, G. S. & Nielsen, R. L. (1993). Comagmat—a Fortran Program to Model Magma Differentiation Processes. *Computers and Geosciences* **19**, 1155–1170.

Ashwal, L. D., Webb, S. J. & Knoper, M. D. (2005). Magmatic stratigraphy in the Bushveld Northern Lobe: continuous geophysical and mineralogical data from the 2950 m Bellevue drillcore. *South African Journal of Geology* **108**, 199–232.

Baker, D. R. & Eggler, D. H. (1987). Compositions of anhydrous and hydrous melts coexisting with plagioclase, augite, and olivine or low-Ca pyroxene from 1 atm to 8 kbar—application to the Aleutian volcanic center of Atka. *American Mineralogist* **72**, 12–28.

Bedard, J. H. (2007). Trace element partitioning coefficients between silicate melts and orthopyroxene: Parameterizations of *D* variations. *Chemical Geology* **244**, 263–303.

Bindeman, I. N., Davis, A. M. & Drake, M. J. (1998). Ion microprobe study of plagioclase–basalt partition experiments at natural concentration levels of trace elements. *Geochimica et Cosmochimica Acta* **62**, 1175–1193.

Blundy, J. D. & Wood, B. J. (1991). Crystal-chemical controls on the partitioning of Sr and Ba between plagioclase feldspar, silicate melts, and hydrothermal solutions. *Geochimica et Cosmochimica Acta* **55**, 193–209.

Boudreau, A. E., Mathez, E. A. & McCallum, I. S. (1986). Halogen geochemistry of the Stillwater and Bushveld Complexes—evidence for transport of the platinum-group elements by Cl-rich fluids. *Journal of Petrology* **27**, 967–986.

Bowes, D. R., Hamidullah, S. & Molyneux, T. G. (1997). Petrochemistry and petrogenesis of the Main and Upper Zones of the Bushveld Complex, Sekhukhuneland, Eastern Transvaal, South Africa. *Utkal University Special Publication in Geology* **2**, 259–282.

Bryan, W. B., Finger, L. W. & Chayes, F. (1969). Estimating proportions in petrographic mixing equations by least-squares approximation. *Science* **163**, 926.

Buchanan, P. C., Koeberl, C. & Reimold, W. U. (1999). Petrogenesis of the Dullstroom Formation, Bushveld Magmatic Province, South Africa. *Contributions to Mineralogy and Petrology* **137**, 133–146.

Buchanan, P. C., Reimold, W. U., Koeberl, C. & Kruger, F. J. (2002). Geochemistry of intermediate to siliceous volcanic rocks of the Rooiberg Group, Bushveld Magmatic Province, South Africa. *Contributions to Mineralogy and Petrology* **144**, 131–143.

Buchanan, P. C., Reimold, W. U., Koeberl, C. & Kruger, F. J. (2004). Rb–Sr and Sm–Nd isotopic compositions of the Rooiberg Group, South Africa: early Bushveld-related volcanism. *Lithos* **75**, 373–388.

Buick, I. S., Maas, R. & Gibson, R. (2001). Precise U–Pb titanite age constraints on the emplacement of the Bushveld Complex, South Africa. *Journal of the Geological Society, London* **158**, 3–6.

Carmichael, I. S. E. (1964). The petrology of Thingmuli, a Tertiary volcano in eastern Iceland. *Journal of Petrology* **5**, 435–460.

Cawthorn, R. G. (2007). Cr and Sr: Keys to parental magmas and processes in the Bushveld Complex, South Africa. *Lithos* **95**, 381–398.

Cawthorn, R. G. & Ashwal, L. D. (2009). Origin of anorthosite and magnetitite layers in the Bushveld Complex, constrained by major element compositions of plagioclase. *Journal of Petrology* **50**, 1607–1637.

Cawthorn, R. G. & McCarthy, T. S. (1985). Incompatible trace-element behavior in the Bushveld Complex. *Economic Geology* **80**, 1016–1026.

Cawthorn, R. G. & Walraven, F. (1998). Emplacement and crystallization time for the Bushveld Complex. *Journal of Petrology* **39**, 1669–1687.

Cawthorn, R. G. & Webb, S. J. (2001). Connectivity between the western and eastern limbs of the Bushveld Complex. *Tectonophysics* **330**, 195–209.

Cawthorn, R. G., Meyer, P. S. & Kruger, F. J. (1991). Major addition of magma at the Pyroxenite Marker in the Western Bushveld Complex, South Africa. *Journal of Petrology* **32**, 739–763.

Clubley-Armstrong, A. R. (1977). The geology of the Selonsriver area, north of Middelburg, Transvaal, with special reference to the structure of the regions southeast of the Dennilton dome. M.Sc. thesis, University of Pretoria.

Daly, R. A. & Molengraaff, G. A. F. (1924). Structural relations of the Bushveld igneous complex, Transvaal. *Journal of Geology* **32**, 1–35.

Dorland, H. C., Beukes, N. J., Gutzmer, J., Evans, D. A. D. & Armstrong, R. A. (2006). Precise SHRIMP U–Pb zircon age constraints on the lower Waterberg and Soutpansberg Groups, South Africa. *South African Journal of Geology* **109**, 139–156.

Dunn, T. & Sen, C. (1994). Mineral/matrix partition coefficients for orthopyroxene, plagioclase, and olivine in basaltic to andesitic systems—a combined analytical and experimental study. *Geochimica et Cosmochimica Acta* **58**, 717–733.

Eriksson, P. G., Hattingh, P. J. & Altermann, W. (1995). An overview of the geology of the Transvaal Sequence and Bushveld Complex, South Africa. *Mineralium Deposita* **30**, 98–111.

Ghiorso, M. S. & Sack, R. O. (1995). Chemical mass-transfer in magmatic processes. 4. A revised and internally consistent thermodynamic model for the interpolation and extrapolation of liquid–solid equilibria in magmatic systems at elevated temperatures and pressures. *Contributions to Mineralogy and Petrology* **119**, 197–212.

Harmer, R. E. & Armstrong, R. A. (2000). Duration of Bushveld Complex (*sensu lato*) magmatism: Constraints from new SHRIMP zircon chronology. *In: National Research Foundation, Bushveld Complex Workshop*, Gethlane Lodge, South Africa, pp. 11–12.

Harmer, R. E. & Sharpe, M. R. (1985). Field relations and strontium isotope systematics of the marginal rocks of the eastern Bushveld Complex. *Economic Geology* **80**, 813–837.

Hatton, C. J. & Schweitzer, J. K. (1995). Evidence for synchronous extrusive and intrusive Bushveld magmatism. *Journal of African Earth Sciences* **21**, 579–594.

Helz, R. T. (1995). The Stillwater Complex, Montana: A subvolcanic magma chamber? *American Mineralogist* **80**, 1343–1346.

Hirschmann, M. M., Ghiorso, M. S., Wasylenki, L. E., Asimow, P. D. & Stolper, E. M. (1998). Calculation of peridotite partial melting from thermodynamic models of minerals and melts. I. Review of methods and comparison with experiments. *Journal of Petrology* **39**, 1091–1115.

Irvine, T. N., Keith, D. W. & Todd, S. G. (1983). The J-M Platinum–Palladium Reef of the Stillwater Complex, Montana. 2. Origin by double-diffusive convective magma mixing and implications for the Bushveld Complex. *Economic Geology* **78**, 1287–1334.

Kruger, F. J. (2005). Filling the Bushveld Complex magma chamber: lateral expansion, roof and floor interaction, magmatic unconformities, and the formation of giant chromitite, PGE and Ti–V–magnetitite deposits. *Mineralium Deposita* **40**, 451–472.

Kruger, F. J., Cawthorn, R. G. & Walsh, K. L. (1987). Strontium isotopic evidence against magma addition in the Upper Zone of the Bushveld Complex. *Earth and Planetary Science Letters* **84**, 51–58.

Lombaard, A. F. (1949). Die geologie van die Bosveldkompleks langs Bloedrivier. (The geology of the Bushveld Complex along Blood River.). *Geological Society of South Africa Transactions* **52**, 343–376.

Lundgaard, K. L., Tegner, C., Cawthorn, R. G., Kruger, F. J. & Wilson, J. R. (2006). Trapped intercumulus liquid in the Main Zone of the eastern Bushveld Complex, South Africa. *Contributions to Mineralogy and Petrology* **151**, 352–369.

Maier, W. D., Arndt, N. T. & Curl, E. A. (2000). Progressive crustal contamination of the Bushveld Complex: evidence from Nd isotopic analyses of the cumulate rocks. *Contributions to Mineralogy and Petrology* **140**, 316–327.

Molyneux, T. G. (1970). The geology of the area in the vicinity of Magnet Heights, eastern Transvaal, with special reference to the magnetic iron ore. *Geological Society of South Africa Special Publication* **1**, 228–241.

Molyneux, T. G. (1974). A geological investigation of the Bushveld Complex in Sekhukhuneland and part of the Steelpoort Valley. *Transactions of the Geological Society of South Africa* **77**, 329–338.

Mondal, S. K. & Mathez, E. A. (2007). Origin of the UG2 chromitite layer, Bushveld Complex. *Journal of Petrology* **48**, 495–510.

Nex, P. A. M., Cawthorn, R. G. & Kinnaird, J. A. (2002). Geochemical effects of magma addition: compositional reversals and decoupling of trends in the Main Zone of the western Bushveld Complex. *Mineralogical Magazine* **66**, 833–856.

Putirka, K., Johnson, M., Kinzler, R., Longhi, J. & Walker, D. (1996). Thermobarometry of mafic igneous rocks based on clinopyroxene–liquid equilibria, 0–30 kbar. *Contributions to Mineralogy and Petrology* **123**, 92–108.

Putirka, K. D., Mikaelian, H., Ryerson, F. & Shaw, H. (2003). New clinopyroxene–liquid thermobarometers for maric, evolved, and volatile-bearing lava compositions, with applications to lavas from Tibet and the Snake River Plain, Idaho. *American Mineralogist* **88**, 1542–1554.

Reynolds, I. M. (1985). The nature and origin of titaniferous magnetite-rich layers in the Upper Zone of the Bushveld Complex: a review and synthesis. *Economic Geology* **80**, 1089–1108.

Richardson, S. H. & Shirey, S. B. (2008). Continental mantle signature of Bushveld magmas and coeval diamonds. *Nature* **453**, 910–913.

SACS. (1980). *Lithostratigraphy of the Republic of South Africa, South West Africa/Namibia and the Republics of Botswana, Transkei, and Venda. South African Geological Survey Handbook* **8**, 690 p.

Saxena, S. K., Sykes, J. & Eriksson, G. (1986). Phase equilibria in the pyroxene quadrilateral. *Journal of Petrology* **27**, 843–852.

Schweitzer, J. K. & Hatton, C. J. (1995). Chemical alteration within the volcanic roof rocks of the Bushveld Complex. *Economic Geology and the Bulletin of the Society of Economic Geologists* **90**, 2218–2231.

Schweitzer, J. K., Hatton, C. J. & de Waal, S. A. (1995*a*). Regional lithochemical stratigraphy of the Rooiberg Group, upper Transvaal Supergroup; a proposed new subdivision. *South African Journal of Geology* **98**, 245–255.

Schweitzer, J. K., Hatton, C. J. & Dewaal, S. A. (1995*b*). Economic potential of the Rooiberg Group—volcanic rocks in the floor and roof of the Bushveld Complex. *Mineralium Deposita* **30**, 168–177.

Schweitzer, J. K., Hatton, C. J. & DeWaal, S. A. (1997). Link between the granitic and volcanic rocks of the Bushveld Complex, South Africa. *Journal of African Earth Sciences* **24**, 95–104.

Scoates, J. S. & Friedman, R. M. (2008). Precise age of the platiniferous Merensky reef, Bushveld Complex, South Africa, by the U–Pb zircon chemical abrasion ID-TIMS technique. *Economic Geology* **103**, 465–471.

Sharpe, M. R. (1981). The chronology of magma influxes to the eastern compartment of the Bushveld Complex as exemplified by its marginal border groups. *Journal of the Geological Society, London* **138**, 307–326.

Sharpe, M. R. (1985). Strontium isotope evidence for preserved density stratification in the Main Zone of the Bushveld Complex, South Africa. *Nature* **316**, 119.

Smith, P. M. & Asimow, P. D. (2005). Adiabat_1ph: A new public front-end to the MELTS, pMELTS, and pHMELTS models. *Geochemistry, Geophysics, Geosystems* **6**, doi:10.1029/2004GC000816.

Tanaka, T. & Masuda, A. (1982). The La–Ce geochronometer—a new dating method. *Nature* **300**, 515–518.

Tegner, C., Cawthorn, R. G. & Kruger, F. J. (2006). Cyclicity in the main and upper zones of the Bushveld Complex, South Africa: Crystallization from a zoned magma sheet. *Journal of Petrology* **47**, 2257–2279.

Toplis, M. J. & Carroll, M. R. (1995). An experimental study of the influence of oxygen fugacity on Fe–Ti oxide stability, phase relations, and mineral–melt equilibria in ferro-basaltic systems. *Journal of Petrology* **36**, 1137–1170.

Twist, D. (1985). Geochemical evolution of the Rooiberg silicic lavas in the Loskop Dam area, southeastern Bushveld. *Economic Geology* **80**, 1153–1165.

Twist, D. & French, B. M. (1983). Voluminous acid volcanism in the Bushveld Complex: A review of the Rooiberg Felsite. *Bulletin of Volcanology* **46**, 225–242.

von Gruenewaldt, G. (1971). A petrological and mineralogical investigation of the rocks of the Bushveld Igneous Complex in the Tauteshoogte–Roossenekal area of the eastern Transvaal. D.Sc. thesis, University of Pretoria.

von Gruenewaldt, G. (1972). The origin of the roof-rocks of the Bushveld Complex between Tauteshoogte and Paardekop in the eastern Transvaal. *Transactions of the Geological Society of South Africa* **76**, 207–227.

von Gruenewaldt, G. (1973). The main and upper zone of the Bushveld Complex in the Roosenekal area, eastern Transvaal. *Transactions of the Geological Society of South Africa* **76**, 207–227.

Wallmach, T., Hatton, C. J., DeWaal, A. & Gibson, R. L. (1995). Retrogressive hydration of calc-silicate xenoliths in the eastern Bushveld complex: Evidence for late magmatic fluid movement. *Journal of African Earth Sciences* **21**, 633–646.

Walraven, F. (1987). *Textural, geochemical, and genetic aspects of the granophyric rocks of the Bushveld Complex. Geological Survey of South Africa Memoir* **72**.

Walraven, F. (1997). *Geochronology of the Rooiberg Group, Transvaal Supergroup, South Africa. Economic Geology Research Unit, University of Witwatersrand, Information Circular* **316.**

Walraven, F. J. (1985). Genetic aspects of the granophyric rocks of the Bushveld Complex. *Economic Geology* **80**, 1166–1180.

Webb, S. J., Cawthorn, R. G., Nguuri, T. & James, D. (2004). Gravity modeling of Bushveld Complex connectivity supported by Southern African seismic experiment results. *South African Journal of Geology* **107**, 207–218.

Wilson, J., Ferre, E. C. & Lespinasse, P. (2000). Repeated tabular injection of high-level alkaline granites in the eastern Bushveld, South Africa. *Journal of the Geological Society, London* **157**, 1077–1088.